Rheological Behaviour of Heptane-Diluted Bitumen in the Presence of Precipitates

by

Zahra Rostami Najafabadi

A thesis submitted in partial fulfillment of the requirements for the degree of

Master of Science

in

Chemical Engineering

Department of Chemical and Materials Engineering

University of Alberta

Abstract

One of the challenges that Vapor Extraction process might be conducted is the unpredictable precipitation of asphaltene from solvent-diluted bitumen that can cause process problems during bitumen extraction in porous media. The objective of this study was to investigate the rheological behaviour of Athabasca bitumen and n-heptane solutions in the present of precipitates using a rheometer and flow through porous media.

Rheometry measurements shown for solutions have the viscosity higher than 0.001 Pa·s and less than 0.0005 Pa·s, the phase angle is around 90° out of phase and the solutions are purely viscous; while for the solutions having the viscosity around 0.0007 Pa·s, the phase angle is around 84° out of phase and the solution behave as a non-Newtonian liquid. Also, the flow of heptane-bitumen solutions through a porous media experiments shows that for bitumen-heptane solution having viscosity around 0.0007 Pa·s, after 24 hours mixing of the solutions, the predicted and measured friction factor did not agreed. This disagreement might be because of both decrease the void area between the particles due to the presence of solids and non-Newtonian behaviour of the solution, which is in consistent with the rheology measurement results.

Acknowledgments

I would like to take this opportunity to express my genuine thank and gratitude to Dr. Anthony Yeung and Dr. Artin Afacan for their bright supervision and inspiring guidance throughout this work. I appreciate their creative ideas which provided a valuable learning experience during this research.

I also would like to thank Dr. Sean Sanders for his permission to use rheometer in his lab.

My deepest thanks goes to my family for their love, support, and being a great encouragement in my life. Special thanks to Farhad, for his endless love and kindness, energy, and support in my graduate experience.

Table of Contents

List of Figures

List of Tables

Nomenclature

D_p Particle diameter (m)

f Frequency (Hz)

f Friction factor

G^* Complex modulus (Pa)

G'' Loss modulus (Pa)

G' Storage modulus (Pa)

L Length (m)

R Universal gas constant (J/mol°K)

R_1 Spindle radius (m)

R_2 Cup radius (m)

Re_{pm} Reynolds number

S Solubility ($MPa^{1/2}$)

T Temperature (°K)

V Molar volume (m^3/mol)

V_s Superficial velocity (m/s)

Greek letters

$\dot{\gamma}$ Shear rate (S^{-1})

γ Surface tension (N/m)

ΔH_v Enthalpy of vaporization (J/mol)

ΔP Pressure drop (Pa)

δ	Phase angle Degree
ε	Porosity
μ	Fluid viscosity (Pa·s)
ρ	Density (kg/m^3)
σ	Shear stress (Pa)
τ	Shear stress (Pa)
ω	Angular velocity (Rad/s)

1 Chapter 1: Introduction

1.1 Oil sands and recovery methods

The depletion of conventional crude oil, has led to a shift towards heavy oil and bitumen to meet the ever-increasing global energy demand. Natural bitumen deposits are reported in many countries including Venezuela, the United States and Russia [1]. In terms of proven global crude oil reserves, Alberta ranks third, after Saudi Arabia and Venezuela. In 2014, Alberta's total proven oil reserves were 170.2 billion barrels, or about 11 % of total global oil reserves. A total of 168 billion barrels or about 99% of Alberta's total oil reserves come from the oil sands, which makes Canada one of the largest sources of bitumen in the world. Oil sands in Alberta cover 142,200 square kilometers in three regions of northern Alberta: Athabasca, Peace River, and Cold Lake [2].

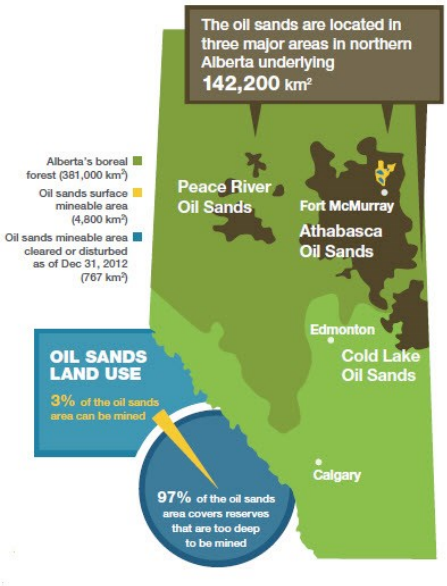

Figure 1-1: Alberta's Oil Sands Areas (OSAs) [2].

Oil sand is a naturally occurring mixture of sand, clay or other minerals, water and bitumen, which is consist of 8-12 wt. % bitumen, 80-85 wt. % solids, and 5-6 wt. % water [3]. Bitumen is an extremely heavy crude oil that contains a large number of hydrocarbon components which are usually fractioned to saturate, aromatic, resins and asphaltenes [4].

The extracted raw bitumen from oil sands, which is extremely viscous oil, must be treated and upgraded (the crude bitumen must first be separated from the sands, other mineral materials and formation water) before it can be used by refineries to produce usable fuels or other petroleum-derived products.

The methods of recovering oil sands are dependent on the depth of the oil sands deposit. Mining the ore is practical when the oil sands deposit is close to the surface (the depth less than 75 m beneath the ground), while deeper deposits are accessed through various in situ technologies such as cyclic steam stimulation (CSS), steam-assisted gravity drainage (SAGD) [3].

In open pit mining, first of all, the overburden on the top of the deposit is removed. Then, the ore is mined with shovels and transported to the bitumen extraction site. Next, the oil sands ore lumps are crushed to smaller sizes and mixed with warm water and chemical additives (e.g. caustic soda) to form oil sand slurry. So, bitumen is dislodged from the sand grains. Mechanical energy in the form of agitation or pipeline transport is introduced into the slurry in order to promote releasing of bitumen. At the same time, air is injected into the slurry to aerate the bitumen droplets. Based on the buoyancy effects, the free, aerated bitumen floats to the top of the gravity separation vessel and forms a froth layer

that can be collected from the top of the vessels. The collected bitumen froth contains roughly 60 wt. % bitumen, 30 wt. % water and 10 wt. % solids [5]. In the next process, froth treatment, the froth must be purified further in order to eliminate the unwanted water and solids from bitumen. Then, the bitumen content is usually more than 99% by weight, which is ready to be sent to upgrading units.

Due to very high viscosity of deeper oil sands deposits, they will not flow under normal reservoir temperature and pressure conditions. By reducing the bitumen viscosity, the bitumen may begin to flow, allowing for production. This process can be done either by increasing the reservoir temperature or injecting solvents. In situ techniques of bitumen extraction can be steam-based (injecting high temperature steam), solvent-based (injecting organic solvent), or mixed co-injection of steam and solvents.

Either cyclic steam stimulation (CSS) or steam assisted gravity drainage (SAGD) is used as the most common thermal techniques by injecting steam into the reservoir. In these methods, thermal energy is applied to heat the bitumen in order to decrease the viscosity, and increase its mobility to pump to the surface through wells using reservoir pressure.

In CSS steam is injected into the reservoir at high temperature and pressure. As the steam condenses, the latent heat from the steam heats the bitumen and reduces its viscosity; then, heated bitumen and condensed steam are transported to the surface [6].

SAGD is a continuous heating and production process that was developed during the late 1970s and early 1980s. In this method, in order to increase the

temperature and reduce the viscosity of bitumen, steam and solvent have been injected into horizontal well drilled through the oil sands deposit. Under the gravity, bitumen with less viscosity flows to the production well where it is transported to the surface [3, 6].

As the use of steam has several disadvantages like consumes large amounts of water, and energy, and produce large amount waste product, which is called tailings. Enhanced oil recovery (EOR) has been the focus of research and development on an alternatives method for bitumen extraction. These techniques include injection of chemicals, gases and solvents into the reservoirs to reduce the interfacial tension, and increasing the mobility of crude oil by reducing its viscosity.

Vapour extraction process is one of the non-thermal alternatives for bitumen production. It starts with the injection of a vaporized hydrocarbon solvent that is close to its dew point into the reservoirs. Solvent diffuses into the bitumen and a significant reduction in viscosity will happen. When a critical concentration of the solvent has diluted the oil, it will begin to flow [6].

After mining, extraction and in situ operations, bitumen is diluted with a light low-viscosity hydrocarbon in order to ship by pipeline to downstream refineries, or it will be upgraded to a higher value synthetic crude oil. Upgrading of bitumen converts it from a viscous oil with low hydrogen and high levels of undesirable elements such as sulphur, nitrogen, oxygen and heavy metals, to a “synthetic” or “upgraded” crude oil having similar characteristics to conventional light sweet crude oil that has a very low sulphur content (0.1 to 0.2 percent). After upgrading,

the synthetic crude oil is shipped through pipelines to refineries for conversion into various petroleum products (gasoline, diesel, etc.).

1.2 Problem statement

Oil sands industries have economic benefits; however, its environmental footprints are not negligible. Today, there are some concerns related to steam-based bitumen extraction such as high energy and water consumption [6]. Water consumption can result in the following environmental problem.

Oil sands extraction consumes large amounts of water. The Athabasca River is the main source of water for oil sands operations, the city of Fort McMurray and neighbouring communities. Current rate of water consumption (170 million cubic metres of water) has negative impact on these communities and ecosystems [7].

Also, enormous amounts of energy required to heat the process water results in problems such as greenhouse gas emissions and depletion of natural gas resources [8].

With increase in oil sands production rate, above mentioned concerns will become more important. So, development of alternative new in situ recovery technologies seems to be a necessity as a substitute for current steam-based method. One of these techniques is VAPEX (Vapour Extraction) [9].

The basic principles of VAPEX technology are similar to SAGD. Both methods involve a horizontal injection well directly above a horizontal production well; however, in VAPEX, a vaporized hydrocarbon solvent is injected instead of steam

as is used in SAGD. In VAPEX, solvent dissolves into the oil near the injection wellbore which results in diluting the oil and decreasing its viscosity [10].

VAPEX process has several features which make it attractive to the petroleum industry. VAPEX process is carried out at reservoir temperature; therefore, the heat loss does not occur. The energy requirements of a VAPEX project are estimated to be approximately 3 % of those for a SAGD project [11]. In addition, with the use of typical separation facilities, some portion of the injected solvent can be recovered [12]. Also, the initial capital expenditure for a VAPEX process can be substantially less than a thermal project. More important, the most attractive feature of VAPEX process is the in situ upgrading of the oil that occurs through asphaltene precipitation, or deasphalting and as a result viscosity of the oil is significantly reduced [13]. However, Unpredictable precipitation of asphaltene, which is high proportion of poorly soluble part of bitumen, might have some effects on rheology and viscosity of diluted bitumen, and as a result might cause some process problems during bitumen extraction in porous media. To develop a practical and successful Vapour Extraction technology, it is essential to find a solution for the above mentioned obstacle before any commercial implementation.

1.3 Objective of present research

One highlighted advantage of solvent-based extraction is the possibility of in-situ upgrading of the oil during the process, since solvent injection makes precipitation of asphaltene. Asphaltene precipitation may take place in the reservoir because of temperature, pressure and compositional changes. In solvent based extraction, the compositional alteration of solvent/bitumen system is the reason for precipitation of asphaltene [14].

The objectives of this study are to determine the rheological behaviour of bitumen /n-heptane solution in the present of asphaltene precipitation using a rheometer (AR-GR) and conduct flow through porous media to confirm this rheological behaviour.

1.4 Thesis structure

The current chapter gives an overall introduction and main objectives of the work done toward this thesis. The chapter 2 will be given information on the basics of characterization of asphaltene, and viscosity as a fundamental physical property of bitumen. It will also provide the theoretical background information on the rheology measurement of bitumen and the fluid flow through porous media. In chapter 3, the focus is on experimental techniques that are used to study the solubility of bitumen in n-heptane, the rheology and viscosity of bitumen-heptane solutions, and the behaviour of diluted bitumen in porous media. The experimental results and discussion are provided in Chapter 4. And finally, the contributions of this research and suggestions for future work are discussed.

2 Chapter 2: Background

2.1 Asphaltene characterization

Asphaltene is considered as the heaviest and most polar component of crude oil that is soluble in aromatic solvents like toluene and insoluble in aliphatic solvents such as n-heptane or n-pentane. The different type of solvents will affect the yield and composition of asphaltene precipitation [15]. Hotier and Robin [16] found that higher-carbon-number n-paraffins could be poorer solvents for petroleum asphaltenes than lower-carbon number n-paraffins. As an example, the molar mass of the asphaltenes precipitated by n-heptane is higher than asphaltenes, which is precipitated by n-pentane [16]. Wiehe et al. [17] have determined that the maximum n-paraffin volume, with increasing n-paraffin carbon number at the onset of asphaltene precipitation is general for crude oils and bitumen. Alboudwarej et al. found that as n-heptane to heavy oil reaches to 40:1 cm^3/g, maximum amount of precipitated asphaltenes were be obtained. Figure 2-1 shows the relationship between the amount of Athabasca asphaltene precipitated and the concentration of n-heptane [18].

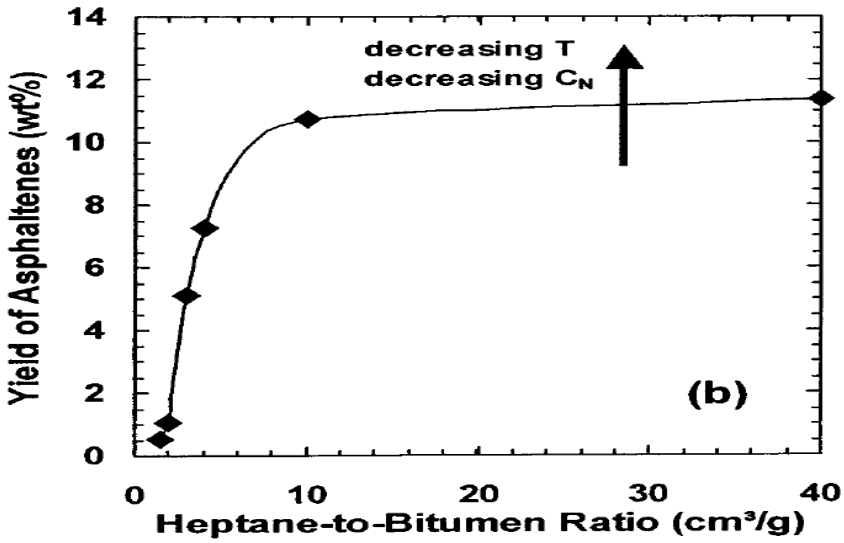

Figure 2-1: Relation between the amount of Athabasca asphaltene precipitated and the concentration of n-heptane [18].

Because of the complex nature of asphaltenes, it is not practical to characterize each molecule within the asphaltenes. In fact, asphaltenes are usually treated as a heterogeneous and the average properties of all the asphaltene components are used to represent the whole asphaltenes. The following sections will give a brief introduction of asphaltenes in terms of elemental composition, molecular weight and structure.

The most basic properties of any chemical compound are its elemental constituents. Chemically, asphaltene contains a high amount of carbons and low hydrogen content. It usually exhibit atomic Hydrogen/carbon (H/C) ratio between 1.42-1.5. This low H/C ratio indicates the highly aromatic nature of asphaltenes. It is also rich in heteroatoms such as sulfur, nitrogen, oxygen as well as some transition metals like vanadium and nickel. The CHNSO elemental composition values (%w/w) for asphaltenes from Alberta heavy oils and bitumen fall in the

range of 80-85% C, 5-12% H, 3.47-8.21% S, 0.94-2.82% N and 0.44-2.61% O [19].

Molecular weight of asphaltenes is the second most important attribute that has received much attention in the literature and is the subject of a significant controversy. Some common experimental techniques used for molecular weight determination such as: vapor pressure osmometry (VPO), mass spectrometry (MS), and fluorescence depolarization (FD). There is a little agreement between the results obtained using these techniques. The results reported to be in the range of 400-10000 Da. However, even for a single technique like VPO, different molecular weights are observed at different temperatures, solvents and asphaltene concentrations. As sphaltenes tend to aggregate in solution even at very low concentrations in aromatic solvent, the large molecular weights reported for asphaltenes from these techniques. It is most likely large molecular weights due to the measurement of aggregate weight, not molecular weight. This aggregation is a well-known property of asphaltenes, which is known to affect measurements, will be discussed later [20].

The molecular structure of asphaltene is a subject of significant debate, especially on the size of the aromatic groups and how they are linked to other structural groups. As asphaltene has a solubility class defined by the fractions of the crude oil, they constitute a wide range of molecule types and functional groups. While the structures in most cases are not known; however, two fundamentally different views of the asphaltenes structure are discussed in the literature. First, the condensed (island) configuration which represents a typical asphaltene molecule

as a core aromatic group with 6-8 fused aromatic rings is surrounded by alkyl chains [21]. Second, the dispersed (archipelago) structure which represents a typical asphaltene molecule as a collection of small aromatic groups linked by aliphatic bridges [22]. Figure 2-2 and Figure 2-3 shows respectively the condensed (island) structure and the dispersed (archipelago) structure.

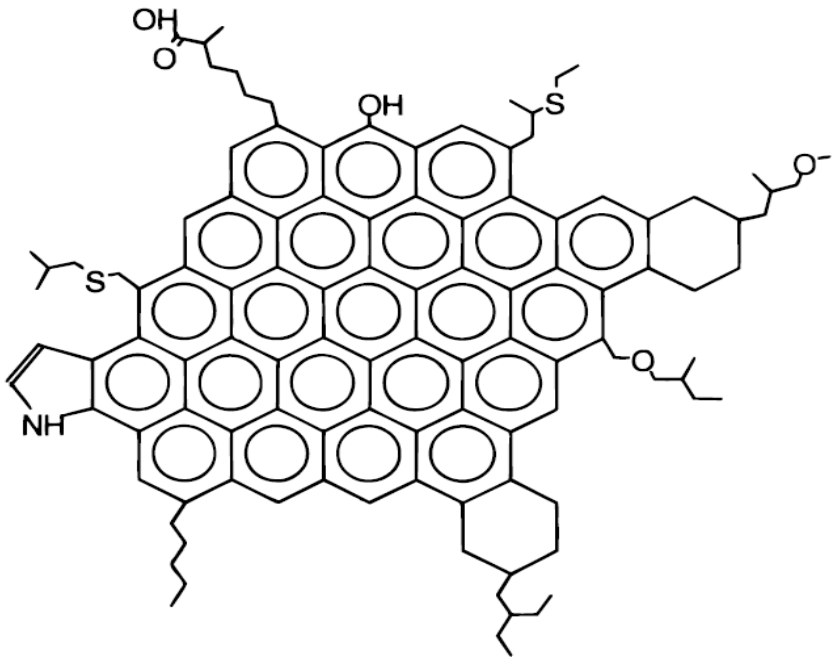

Figure 2-2: Hypothetical condensed asphaltene molecular structure [21].

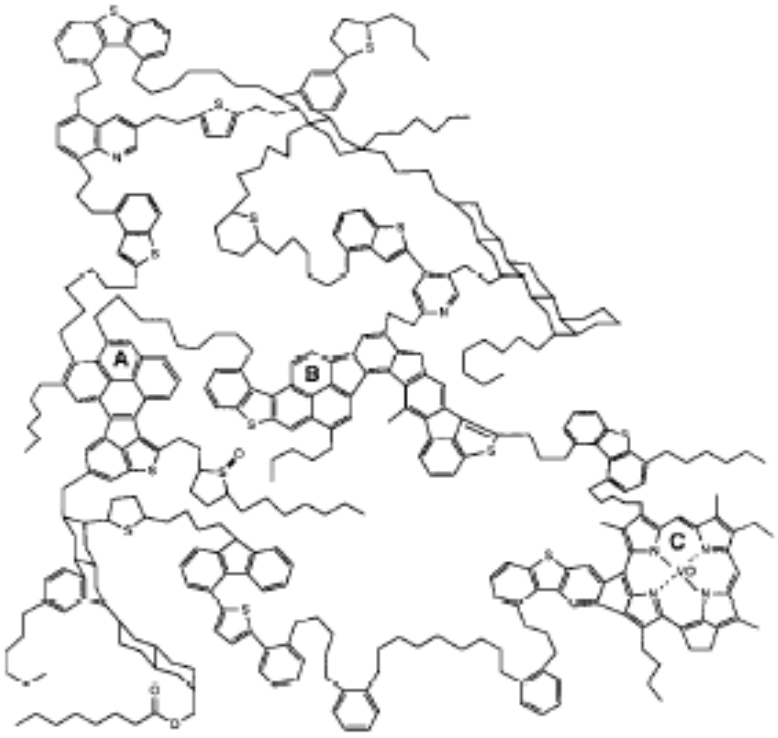

Figure 2-3: A hypothetical dispersed asphaltene molecular structure [22].

2.2 Asphaltene flocculation and precipitation

Asphaltene aggregation is the initial step towards precipitation. Asphaltene aggregates will flocculate to form larger clusters and precipitate out of the solution. Upon changes in crude oil composition, pressure and temperature, asphaltene precipitation will be affected. For example, when the oil becomes less aromatic due to the addition of gases or paraffinic solvents may result in precipitation. For example, when heavy oils or bitumen diluted with condensates, distillation cuts (naphtha) or light oil, which are usually rich in paraffinic, to reduce the viscosity for processing and transport may result in precipitation. Increasing temperature can increase the solubility of asphaltenes and therefore

reduce their amount precipitated. Also, Depressurization of crude oil can also induce asphaltene precipitation [23].

The condition, which is important in asphaltene precipitation, is the point where asphaltene begins to precipitate. This point which is called onset of asphaltene precipitation or flocculation is defined as the minimum amount of precipitant necessary to induce the precipitation of solids. There are some methods to determine the precipitation onset. At atmospheric conditions, the most common method to determine the precipitation onset is the titration of oil against the precipitating solvents [24].

At the bubble point, the oil has the highest content of dissolved gas by volume, so the maximum amount of asphaltene precipitation will occur [25]. Below the bubble point, solution gas and other volatile components will evolve from the oil as a gas phase. It will become a better solvent for the asphaltenes in the liquid phase. Therefore, the precipitated asphaltenes will start to redissolve into the oil. The pressure at which the last of the precipitated asphaltenes redissolve is called the lower asphaltene precipitation onset pressure. At atmospheric conditions, filtration and centrifugation is usually using for measuring amount of precipitation. In these techniques, the oil is mixed with an appropriate solvent and filtered or centrifuged [26].

There is still disagreement in the open literature as to the state of asphaltenes in oil and their flocculation mechanisms. True state of asphaltenes in the crude oil and the mechanism of their flocculation are important. Depending on the hydrocarbons present and the relative amounts of each family of heavy organics

in oil, the type and amount of depositions of heavy organics from petroleum fluids will vary. In the following, four different mechanisms will be reviewed [27].

Aggregation effect

Variation of a peptizing agent concentration such as resins in oil, which is particularly important in colloid chemistry for precipitation reactions in an aqueous solution, will change its adsorbed amount on the surfaces of heavy organic particles. When the peptizing agent concentration in oil is low, then its adsorbed amount would not be high enough to cover the entire surface of heavy organic particles. So, this may cause irreversible aggregation. Heavy organic particles will come together, and then they will grow in size, and flocculate [27].

Poly-dispersivity effect

Deposition of heavy organics can be explained by an upset in the polydisperse balance of oil composition. The dispersion degree of heavy organics in oil depends on the chemical composition of petroleum. Factors which play an important role in stability of polydisperse oil mixture are the ratio of polar/non-polar and light/heavy molecules and particles in petroleum. Differentiate in temperature, pressure, and composition may destabilize the polydisperse oil. For example, by addition of a polar miscible solvent to oil, which increases the aromatic hydrocarbon content of a crude oil, asphaltene particles form micelle-type aggregates. It is due to packing constraints, resulting from the complicated molecular structure of asphaltene. Also, upon increase in the paraffinic

hydrocarbon content of a crude oil, asphaltene particles may separate into a solid aggregate phase. Segments of the separated fractions which contain sulfur, nitrogen, oxygen and/or hydrogen bonds could start to flocculate and as a result produce the irreversible heavy organic deposits which may be insoluble in solvents [27].

Steric colloidal effects

As it is mentioned before, some of the components of petroleum, especially asphaltene have a strong tendency for self-association. By increasing of the paraffinic hydrocarbon content of a crude oil some of the heavy organics will form colloids. They will separate from the oil phase into an aggregate and remain suspended in oil by some peptizing agents, like resins that will be adsorbed on their surface and keep them afloat.

Stability of steric colloids is depended on the concentration of the peptizing agent in the solution, the fraction of heavy organic particles surface sites occupied by the peptizing agent, and the equilibrium conditions between the peptizing agent in solution and on surface of heavy organic particles [27].

Electrokinetic effect

When oil is flowing in porous medium, well, pipeline and etc., electrokinetic effect is an additional effect to be considered in the deposition of its colloidal heavy organic constituents due to development of an electrical potential difference along the length of the conduit generated by the motion of charged

colloidal particles. This electrical potential difference can cause change in the charged and colloidal particles further down the conduit. So, they will sediment and plugging of the conduit.

Temperature, pressure, electrical, thermal and wettability characteristics of the conduit, flow regime, flowing oil properties, characteristics of the polar heavy organics and colloidal particles, and blending of the oil are the factors that influence electrokinetic effect.

One or more of the effects described above will cause heavy organic depositions, depending on the operation and the kind of heavy organics present in the oil [27].

Asphaltene precipitation will be affected by change in pressure and temperature during production. In the following the effect of temperature on asphaltene precipitation will be reviewed.

Different trends have been reported in the influence of temperature on asphaltene yield. It is commonly noted that with increasing reaction temperature, the asphaltene yield mainly by n-propane treatment increases contrary to most other types of solvent extracting processes [16]. However, a massive number of reports illustrate with increasing temperature using n-alkanes with carbon number above 5, the precipitated amount of asphaltene will decrease [28]. Figure 2-4 shows an initial increase in asphaltene yield followed by a decrease using different solvents, leading to maximum precipitation at a certain temperature [29].

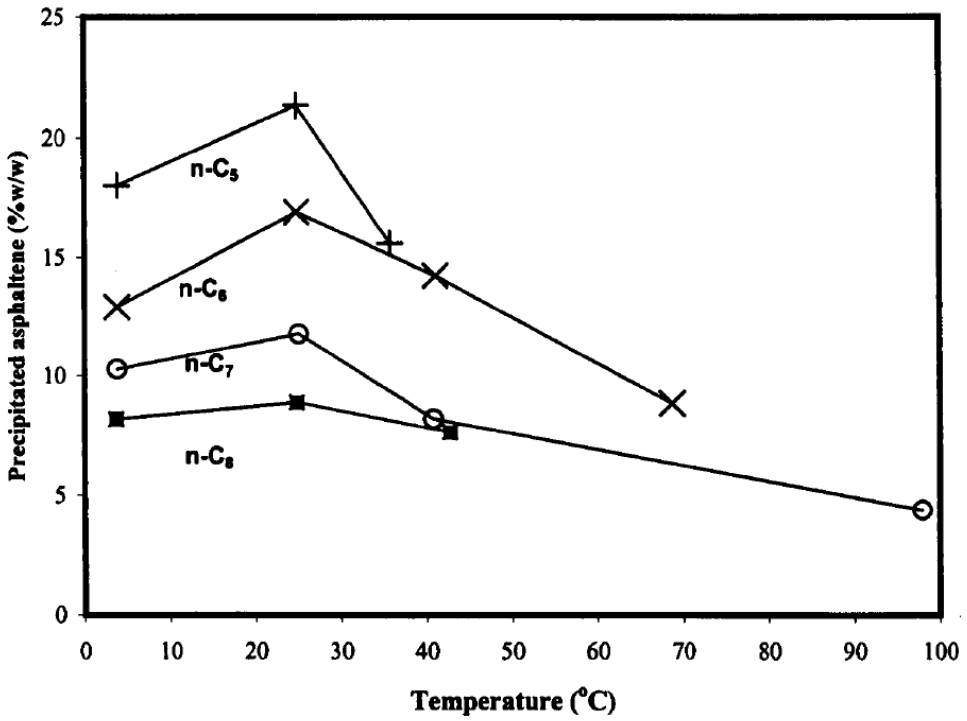

Figure 2-4: Precipitated asphaltenes (%w/w) vs. temperature using n-C5 to n-C8 [29].

As shown in Figure2-4, for all n-alkanes the precipitation curves exhibit a maximum at 25°C and it is more pronounced as the carbon number decreases. This demonstrates a dependence of the temperature effect on the actual carbon number of the precipitant [29]. However, the temperature has been found to significantly affect the composition of the asphaltenes, which is in accordance with the description of asphaltene precipitation. Andersen [30] conducted several separation experiments in order to address the effect of temperature on the amount and the composition of asphaltene. He used Boscan and Kuwait crude oils by n-heptane at constant temperatures ranging from -2 to 80°C. The results of his experiments have showed that the yield of asphaltenes is decreased with increasing precipitation temperature for both samples as shown Figure 2-5.

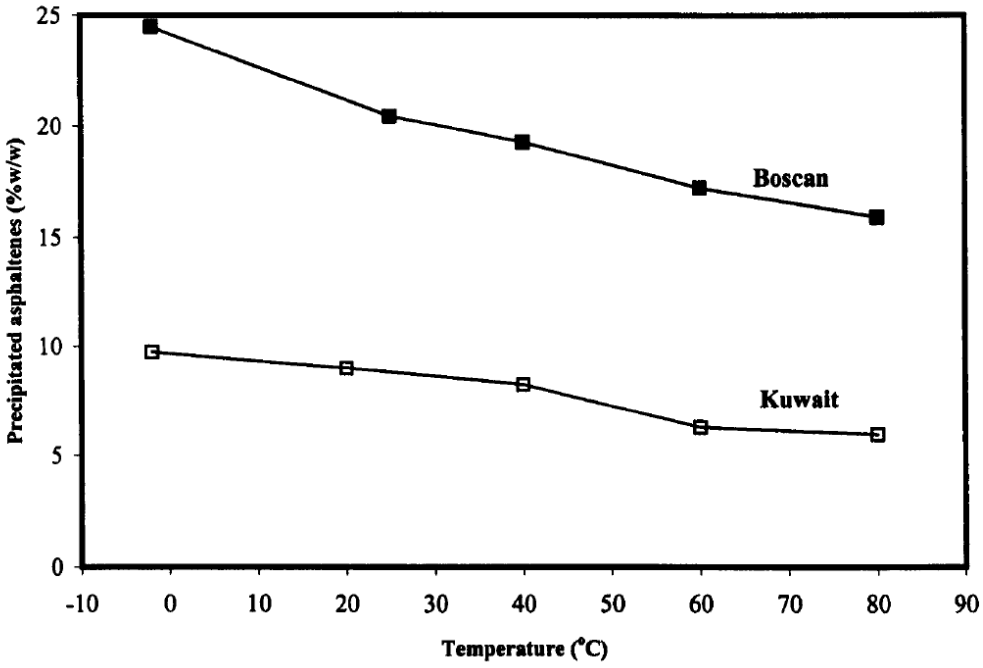

Figure 2-5: Effect of temperature on n-heptane asphaltene precipitated [30].

He observed that with increased temperature the asphaltenes have lower H/C and higher apparent molecular weight which means they are more aromatic. So, the remaining material in solution has a higher H/C ratio, which indicates a higher solubility in n-heptane. He believes that asphaltene precipitation may not be sensitive to temperature, and that temperature may increase or may decrease the onset of asphaltene precipitation.

2.3 Properties

Accurate physical and transport properties for bitumen and heavy oil are key parameters for the oil industry. Viscosity is a fundamental physical property of bitumen, because of its use in design calculation and its use in estimation of other

transport propertied. Also, density and solubility parameters of bitumen are two important thermodynamic properties which all are reviewed in the following.

2.3.1 Density

The density of asphaltenes is normally used to obtain by gravimetric measurements. The density of solid asphaltenes from crude oil was reported to be between 1170 and 1280 kg/m³ [19]. The density of asphaltenes which is more aromatic (smaller H/C ratio) is larger than the asphaltenes which has a larger H/C ratio. Yarranton and Masliyah [31] measured the densities of solutions of different concentrations of asphaltenes in toluene. They reported the density of asphaltene in ranged of 1100 to 1200 kg/m³.

2.3.2 Solubility Parameter

The most accepted empirical thermodynamic approach to describe asphaltene stability is the solubility parameter. The solubility of asphaltenes is of interest to the oil industry because asphaltenes can precipitate during oil production, reducing flow rates and fouling equipment. The amount of precipitated asphaltenes from Athabasca bitumen is correlated linearly with the solubility parameter of the solvent (S).

Hildebrand et al [19] proposed the following equation to calculate the cohesive energy density as:

$$S = \gamma V^{-\frac{1}{3}} \tag{2.1}$$

Where, γ is the surface tension, V is the molar volume at a given pressure and temperature. The most used expression for solubility parameter, at temperatures below the normal boiling point and low pressures is given by [19]:

$$S = \sqrt{\frac{\Delta H_v - RT}{V}} \tag{2.2}$$

Where ΔH_v is the enthalpy of vaporization (J/mol), R is the universal gas constant (8.314 J/mol °K), v is the molar volume (cm^3/mol), and T is the absolute temperature (ºK). For these units, the solubility parameter is reported in $MPa^{1/2}$ in SI.

This Equation shows that solvents with enough energy of solution to overcome the association forces between the asphaltene aggregates are capable of dissolving asphaltenes. n-heptane is the most widely used solvent for the precipitation of asphaltenes. Propane and n-pentane are also common, especially for industrial scale applications. More precipitation of asphaltenes is the results of solvents with lower solubility parameters. For example propane with the solubility of 13.1 $MPa^{1/2}$ can separate more asphaltenes than n-pentane with the solubility of 14.4 $MPa^{1/2}$. Also, n-pentane precipitates more than n-heptane (S = 15.3 $MPa^{1/2}$).

Hansen [19] provided a complete list of solubility parameter data for most of the pure components. The solubility parameters for pure components are calculated for a given pressure and temperature by using measured data for enthalpy of vaporization which is available in the literature for pure components. For unknown compounds, solubility parameter can be obtained by measuring the heat

of vaporization, vapor pressure, boiling point, heat of mixing and internal pressure.

Characterization and prediction of asphaltenes solubility is difficult rather than a pure compound because it has a solubility class. Recently, more accurate results were obtained when the asphaltenes were treated as a multi-component mixture with a variety of physical properties. However, the determination of solubility parameters of asphaltenes is uncertain due to their operational definition. Hirschberg et al. [32] reported the solubility parameter of asphaltenes for temperature dependence as 19.50±0.5 $MPa^{1/2}$. Lian et al. [33] used the miscibility of asphaltenes in various solvents to report the solubility parameter values ranging from 17.6 to 21.3±0.5 $MPa^{1/2}$. Yarranton and Masliyah [31] determined the solubility parameter to be in the range of 19 to 21±0.5 $MPa^{1/2}$ by fitting their solubility model to asphaltene-toluene-n-heptane solubility data.

2.3.3 Viscosity

As bitumen and heavy oils are asphaltene-rich complex hydro carbon mixtures, they make various challenges during production, transport, and refining. The high viscosity of these hydrocarbon resources is attributed to their asphaltene content and to asphaltene-maltene interactions. So, effective viscosity of bitumen in the presence of asphaltene has been studied extensively for the past several decades. For example, Hasan et al. [34] showed that the viscosity of deasphalted oil was up to several hundred times lower than the viscosity of mixtures that are comprised of up to 20 volume percent asphaltenes plus parent oil. However, most of the

available data focus on the dependence of viscosity on external factors such as pressure, temperature, and the presence of various additives, such as diluents (benzene, toluene, n-alkane, etc.), and dissolved gases (CO2, N2, CH4, C2H6, etc) [34].

2.4 Bitumen rheology and viscosity Background

2.4.1 Newtonian and non-Newtonian fluids

"Rheology" was first formulized by Isaac Newton [35]. He observed that some liquids could be made to flow more easily than others; also, the flow rate of each material depended on the force to which they were applied. These observations are now more formally described by stress (σ) and strain (γ). When shear stress is applied to a fluid it will suffer a continuous deformation, which is referred to as "flow". Stress is the force acting on a sample per unit area and strain is the amount of deformation in response to the applied stress as shown in Figure 2-6.

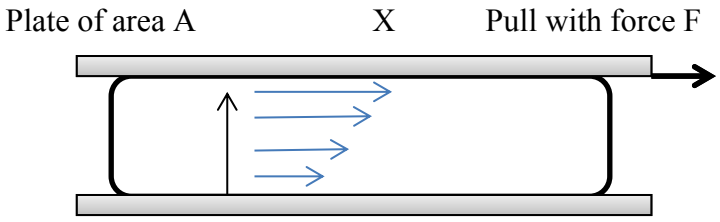

Figure 2-6: Definition diagram for shear deformation

Where σ (stress) is force per unit area, expressed as Pa; Also, γ (shear strain) is relative deformation in shear (no units), and $\dot{\gamma}$ (Shear rate) is change of shear strain per unit time, expressed as s^{-1}.

Fluid viscosity (μ) is the property, which indicates the fluid's resistance to flow due to an unbalanced shearing force. As shown in Figure 2-6, viscosity can be mathematically expressed as the ratio between the shear stress and the shear rate. From the expression described above, fluids can be classified as either Newtonian or non-Newtonian. A Newtonian fluid is a fluid that the viscosity throughout the fluid is independent of strain rate. The constant of proportionality is called the coefficient of viscosity [35]. The plot of shear stress versus strain rate for Newtonian fluids yields a straight line with a slope of μ, is shown in Figure 2-7.

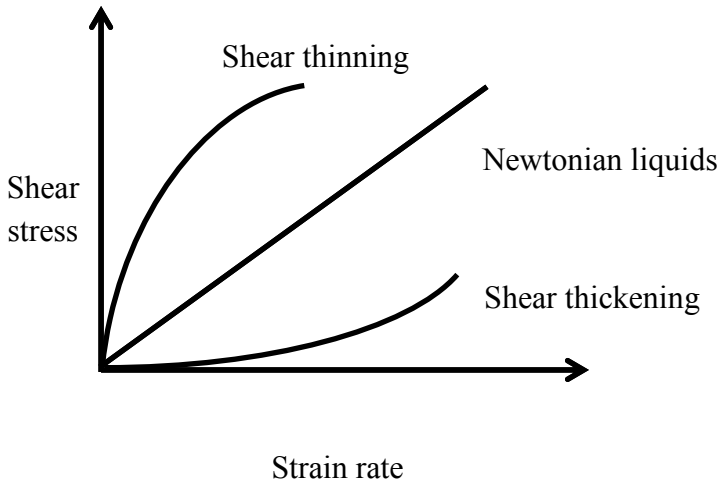

Figure 2-7: Flow curves showing Newtonian and non-Newtonian fluid behaviours

At some condition the linear relationship between shear stress and shear rate no longer holds and viscosity will dependent on the strain rate. These fluids are

known as non-Newtonian fluids, which can be subcategorized in to time dependent liquids and time independent liquid.

1) Non-Newtonian time independent liquids: in this type of fluids, the viscosity of a fluid is dependent on the shear rate but independent of the time of shearing. These fluids include shear thinning or pseudo-plasticity and shear thickening or dilatancy. In shear thinning fluids viscosity decrease with increasing shear rate, and in shear thickening, viscosity increase with increasing shear rate. A typical flow curve is shown in Figure 2-7.

2) Non-Newtonian time dependent liquids: in this type of fluids, the viscosity of a fluid is dependent on the both shear rate and the time of shearing. Such fluids can be described as thixotropic, a decrease in viscosity with time under a constant shear rate or shear stress followed by a gradual recovery when the force is removed; and rheopectic, an increase in viscosity with time under constant shear rate or shear stress followed by a gradual recovery when the force is removed [35].

There is a massive amount of literature on Athabasca bitumen viscosity. It is well documented that bitumen viscosity is very sensitive to factors such as temperature, solvent residue concentration, and asphaltene content. These factors can be summarized into two categories. First category is bitumen composition which involves sample sources, sample aging and contamination, solvent residue in the samples, and hard to control. Second category is physical alteration which can be comparatively well manipulated in the laboratory, and include extraction

and evaporation methods, experimental temperature and pressure, equipment and geometry, and analytical procedure. However, for the same sample viscosity measured at an equivalent temperature can be different. For example, the studies by Wallace et al. [36] and Moran and Yeung [37] on Syncrude coker feed show a difference in the measured viscosity. Wallace et al. [36] used a Brookfield cone and plate viscometer, while Moran and Yeung [40] used a drop shape recovery method. Also, Hasan et al. [34] displayed that measurement of bitumen viscosity is affected by differences in the oil sand ore source, the bitumen extraction and post-extraction processes, rheological instrumentation applied and operating parameters.

Bitumen is a thermoplastic liquid that behaves as a viscoelastic material. The term viscoelastic behaviour refers to the mechanical properties of the bitumen, can result in the bitumen behaving either as an elastic solid or a viscous liquid, depending on temperature and time of loading. Changes to the asphaltene aggregate structure, asphaltene-maltene interaction, and asphaltene self-association are other parameters which contribute to the temperature dependence on bitumen viscosity. At low temperatures elastic properties dominate. At high temperatures, the bitumen behaves like a liquid, usually with Newtonian viscous flow properties [38]. Ward and Clark [39] have used pressure driven capillary viscometer in studying of several Athabasca bitumen samples which were collected from different sites, and have illustrated Newtonian behaviour for bitumen at 29.1 °C. Dealy [40] studied bitumen extracted from Athabasca, and Cold Lake and he concluded that bitumen displayed some degree of non-

Newtonian behaviour at 27.5 °C. He also observed that the onset of shear-thinning occurs between low shear rates of 0.1 to 1 s^{-1}. In addition, he detected 10% reduction in viscosity for all the samples due to asphaltene molecular aggregation and de-aggregation. Hasan et al. [34] using a rotational rheometer to assess the rheological properties of Athabasca bitumen and they observed Newtonian behaviour at 25 °C.

2.4.2 Rheology

2.4.2.1 Dynamic mechanical analysis for Newtonian behaviour

Capillary-pipe flow testing and rotational rheometry are two other common techniques for measurement of fluid rheology. Rotational rheometry is a particularly effective technique for measuring viscosity and rheology of Newtonian materials. In this method, different type of geometries such as cone and plate, parallel plate, and concentric cylinder configurations can be applied to measure viscosity. Cone and plate and parallel plate geometries are not suitable for the measurement of slurry rheological behaviour when larger particles or aggregates are present due to settle larger particles during testing and the resulting concentration gradient gives the appearance of lower slurry viscosity. In order to measure rheological behaviour, Shook et al mentioned that ideally particles do not settler or at least must settle slowly. Concentric cylinder is most suitable geometry for the relatively low viscosities and for samples with having precipitate due to reduce sedimentation. It operates on the principles of Couette flow [41]. For this geometry, bob is allowed to freely rotate within a fixed cup while the speed of the

bob is controllable, and the torque response is measured. A schematic illustration of a concentric cylinder rheometer is shown in Figure 2-8. Where the R1 is the bob radius, R2 is the cup radius, and L is the length of the bob in the field of measurement all in (m). The angular velocity or bob speed of the system is given by ω (rad/s).

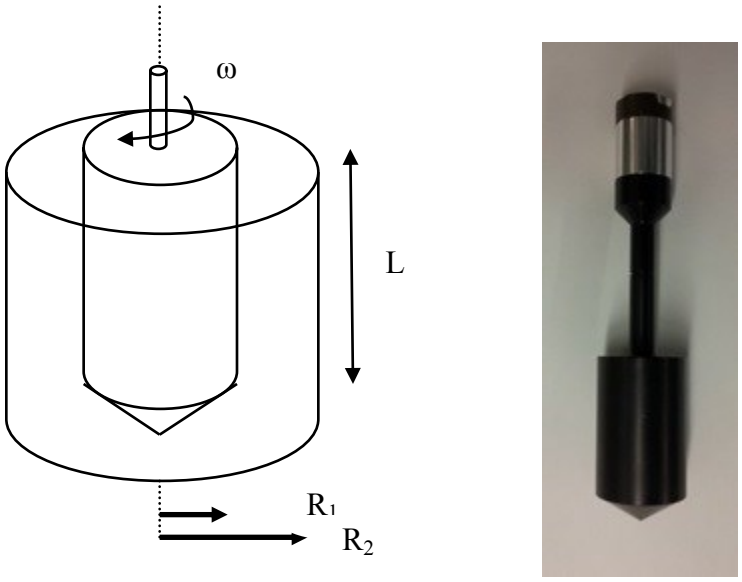

Figure 2-8: (a) Schematic illustration of a concentric cylinder rheometer; (b) Schematic illustration of a bob of AR-G2 rheometer

Samples must be sheared at low enough speeds, which laminar fluid flow occurs, to obtain meaningful results. Otherwise, at excessively high speeds Taylor vortices may occur [42]. In this case, results would be higher than true values for the material. Care must be taken to ensure all measured data are analyzed only at spindle speeds where the sample is fully sheared and only laminar (viscous) flow occurs.

Newtonian fluid behaviour is characterized by a linear relationship between shear rate and shear stress for a fluid exhibiting no yield stress as shown earlier in Figure 2-7. Newtonian viscosity is the ratio of Shear stress to shear rate and can be calculated by [42],

$$\tau = \mu\dot{\gamma} \tag{2.3}$$

Where τ is shear stress (Pa), μ is the viscosity (Pa·s), and $\dot{\gamma}$ is shear rate (1/s).

For concentric cylinder rheology measurements, this relationship can also be expressed in terms of angular velocity (spindle speed) ω and torque T as [43] as:

$$\omega = \frac{T}{4\pi L\mu}\left[\frac{1}{R_1^2} - \frac{1}{R_2^2}\right] \tag{2.4}$$

Where ω is the maximum angular velocity for Newtonian fluid (rad/s) and can be calculated by [44]

$$\omega_{critical} = \frac{45\mu}{\left[\frac{(R_1 + R_2)^{1/2}}{2}\right](R_2 - R_1)^{3/2}\rho} \tag{2.5}$$

2.4.2.2 Dynamic mechanical analysis for non-Newtonian behaviour

Various forms of dynamic mechanical analysis (DMA) are used to measure the rheological properties of bitumen by oscillatory type (DSR) testing. The principle used with the DSR is to apply sinusoidal, oscillatory stresses and strains to a thin disc of bitumen, which is sandwiched between the two parallel plates. The test can be either stress or strain-controlled, depending on which of these variables is

controlled by the test apparatus. The controlled-strain test is normally used to determine the dynamic rheological properties of the bitumen [45].

The sinusoidally varying stress can be calculated as:

$$\sigma(t) = \sigma_0 \sin \omega t \tag{2.6}$$

and the resulting strain can be obtained by

$$\gamma(t) = \gamma_0 \sin(\omega t + \delta) \tag{2.7}$$

Where σ_0 is the peak stress (Pa), γ_0 is the peak strain, ω is the angular frequency (rad/s), t is the time (s) and δ is the phase angle (°) of the measured material response. The angular frequency, ω, also known as the rotational frequency, is expressed as

$$\omega = 2\pi \, \mathrm{f} \tag{2.8}$$

Where f is the frequency (Hz) at which the test was conducted.

The phase angle, δ is important in describing the viscoelastic properties of materials. It is defined as the phase difference between stress and strain. For purely elastic materials, the phase angle will be 0º out of phase, while for purely viscous materials; the phase angle will be 90º out of phase. The sinusoidal, oscillatory, stress and strain waveforms and the resulting dynamic test outputs are shown in Figure 2-9.

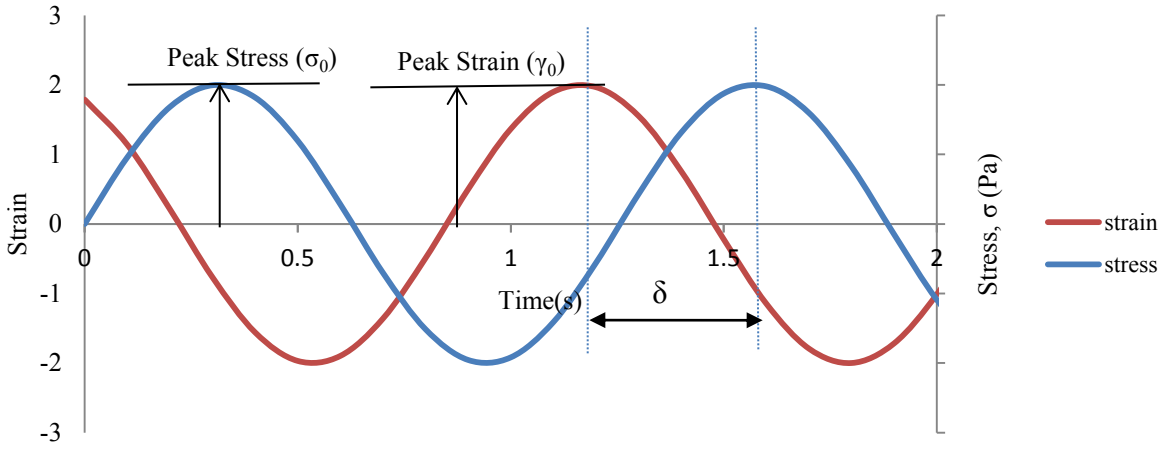

Figure 2-9: Dynamic oscillatory stress-strain functions

The ratio of the resulting stress to the applied strain is called the complex shear modulus, G*, defined as

$$G^* = \left(\frac{\sigma_0}{\gamma_0}\right)\cos\delta + i\left(\frac{\sigma_0}{\gamma_0}\right)\sin\delta \qquad (2.9)$$

G* can also be defined in terms of G' and G"

$$G^* = G' + iG'' \qquad (2.10)$$

Where G' is the storage modulus (Pa) which is the stress at 0 degree divided by peak strain, G" is the loss modulus (Pa) which is the stress at 90 degree divided by peak strain, and i is the imaginary unit, which is defined solely by the property that its i^2 is −1.

The storage modulus describes the amount of the energy that is stored and released elastically in each oscillation and is therefore also known as the elastic modulus, or the elastic component of the complex modulus.

$$G' = G^* \cos\delta \tag{2.11}$$

The loss modulus describes the average energy dissipation rate in the continuous steady oscillation found in the dynamic test. The loss modulus is also referred to as the viscous modulus or the viscous component of the complex modulus.

$$G'' = G^* \sin\delta \tag{2.12}$$

The loss tangent is defined as the ratio of the viscous and elastic components of the complex modulus or simply the tangent of the phase angle [45]:

$$\delta = \tan^{-1}\frac{G''}{G'} \tag{2.13}$$

Figure 2-10 shows a relationship between *G*, G′, G″ and δ*.

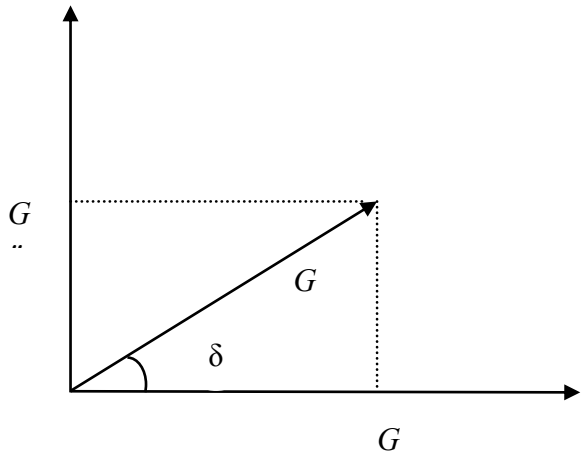

Figure 2-10: Relationship between *G**, *G′*, *G″* and δ [45]

2.5 Fluid flow in porous media

There have been two main approaches for developing friction factor expression for packed columns. In one method the packed column is visualized as a bundle of tangled tubes of wired cross section; the theory is then developed by applying the equation for single straight tubes to the collection of crooked tubes. In the second method the packed column is regarded as a collection of submerged objects, and the pressure drop is obtained by summing up the resistance of the submerged particles. The tube bundle theories have been somewhat more successful, and summarized in most chemical engineering texts or journals on fluid mechanics or transport phenomena [42, 46, 47].

For a packed bed of spherical particles, the experimental friction factor can be calculated by

$$f = \left[\frac{\Delta P}{L}\right]\left[\frac{D_P}{\rho_f V^2}\right]\left[\frac{\varepsilon^3}{1-\varepsilon}\right] \tag{2-14}$$

Where the f is the friction factor, ΔP is the pressure drop (Pa), L is the length of the column (m), D_p is the particle diameter (m), ρ_f is the fluid density (kg/m^3), V is superficial velocity (m/s), and ε is the porosity.

A variety of equations have been proposed for flow in packed beds of spheres over various Reynolds number, Re_{Pm} ranges. Ergun (1952) [48] has developed an empirical expression for predicting friction factor for Reynolds number ranges between 1 and 1000 in the following form:

$$f = \frac{150}{\mathrm{Re}_{Pm}} + 1.75 \tag{2-15}$$

Where the Reynolds number, Re_{Pm}, is defined as**:**

$$\mathrm{Re}_{Pm} = \frac{D_P V \rho_f}{\mu(1-\varepsilon)} \tag{2-16}$$

Where the μ is the viscosity (Pa·s), D_p is the particle diameter (m), ρ_f is the fluid density (kg/m^3), V is superficial velocity (m/s), and ε is the porosity.

Ergun's equation is a combination of the laminar and turbulent components of the pressure gradient. Under laminar conditions where the Re_{Pm} number is less than 10, the first term in equation (2-15) dominate. In laminar flow, the pressure gradient increases linearly with superficial fluid velocity and independent of fluid density. Under turbulent flow, where the Re_{Pm} number higher than 1000, the second term dominates. The pressure gradient increases as the square of superficial fluid velocity and is independent of fluid viscosity.

3 Chapter 3: Experimental work

Bitumen can be dissolved in aromatic solvents. However, when bitumen is mixed with an alkane solvent, such as heptane, it is divided roughly into two components: asphaltenes and maltenes. Asphaltene is the part that is not soluble in an aliphatic solvent and it contains the highest molecular weight components of bitumen. Maltene is the part that is soluble in an aliphatic solvent and it consists of moderate to low molecular weight components such as resins, aromatics and saturates. The amount of precipitated asphaltene depends on the bitumen to solvent ratio and on the carbon number of the alkane solvent being used.

For all tests, Athabasca bitumen obtained from Syncrude Canada Ltd was diluted using HPLC grade n-heptane purchased from Fisher Scientific. In part of our study, the method we used for assessing the solubility of bitumen in n-heptane is as follows: HPLC grade n-heptane diluted bitumen and bitumen solutions at 1:5, 1:10, 1:20, 1:40, 1:60, 1:80, 1:200 wt. % ratios (bitumen: n-heptane) were prepared. To ensure that the mixture was completely mixed and most of asphaltene was precipitated, the mixture was mixed using a magnetic stirrer for an hour. Teflon bottles (NALGENE Labware, FEP material) were used for all preparation steps to minimize the attachment of bitumen and precipitated asphaltene to the container walls. Once samples were prepared, the mixtures were filtered using porcelain Buchner funnels (purchased from Fisher Scientific) under vacuum to separate both soluble and insoluble part of bitumen in n-heptane. In filtration step, Whatman quantitative filter paper, ash less grades with 25μm pore size was utilized. The deposited bitumen on filter paper was dried under a fume

hood for 2 days and weighed. It was found that the filtrate yield from Athabasca bitumen is affected by heptane-to-bitumen ratio.

3.1 Rheology measurements

All samples, which were used for rheology tests were the same as samples for solubility test. n- heptane-diluted bitumen solution at 1:1, 1:5, 1:10, 1:20, 1:40, 1:60, 1:80, and 1:200 wt. % ratios (bitumen: n-heptane) were prepared and the mixture was mixed by a magnetic stirrer for an hour. Rheological measurements were conducted using a controlled stress / direct strain / controlled rate rheometer (AR-G2). This rheometer contains concentric cylinder, parallel plate, and cone and plate. It has minimum 1.4E-9 rad/s and maximum 300 rad/s rotational speeds. Controlled rate operation torque response can be measured in the range of 0.01 μNm to 200 mNm with a resolution of 0.1 nNm. The liquid sample temperature was controlled using external re-circulating fluid bath utilizing de-ionized water as the heating/cooling medium. In this study, the concentric cylinder measurement system was selected for testing because; it is most suitable geometry for the relatively low viscosities and for samples with having precipitate due to sedimentation. A photographic illustration and detail dimensions of the rheometer are provided in Figure 3-1 and Table 3-1 respectively.

Figure 3-1: Cylinder geometry rheometer (from TA Instruments, 2014)

Table 3-1: Specifications of AR-G2 concentric cylinder geometry

Geometry	**Concentric Cylinder with DIN Rotor**
Cup Diameter (mm)	30.40
Rotor Diameter (mm)	28.00
Rotor Length (mm)	42.03
Minimum Sample (mL)	22.42
Operating Gap (mm)	0.010

Before measuring the rheological properties of bitumen-heptane solutions, the rheometer was calibrated with deionised water and standard Newtonian oils. The viscosities were obtained at 25°C under rotational mapping mode with angular velocity range of 0.5 to 8 rad/s to keep the flow in laminar regime. Furthermore, for all measurement, the oscillation mapping mode was used at 0.05 Hz frequency

and 1.5 rad displacement to apply sinusoidal, oscillatory stresses and strains to a thin disc of liquid, which was sandwiched between the two parallel plates to determine the dynamic rheological properties of the liquid. Figure 3-2, Figure 3-3 and Figure 3-4 show the measured shear stress versus shear rate for deionized water, N100 and S200 standard oil samples. It can be seen that for all three Newtonian fluids, as shear rate increases the shear stress increases linearly as expected. This is a typical Newtonian behaviour.

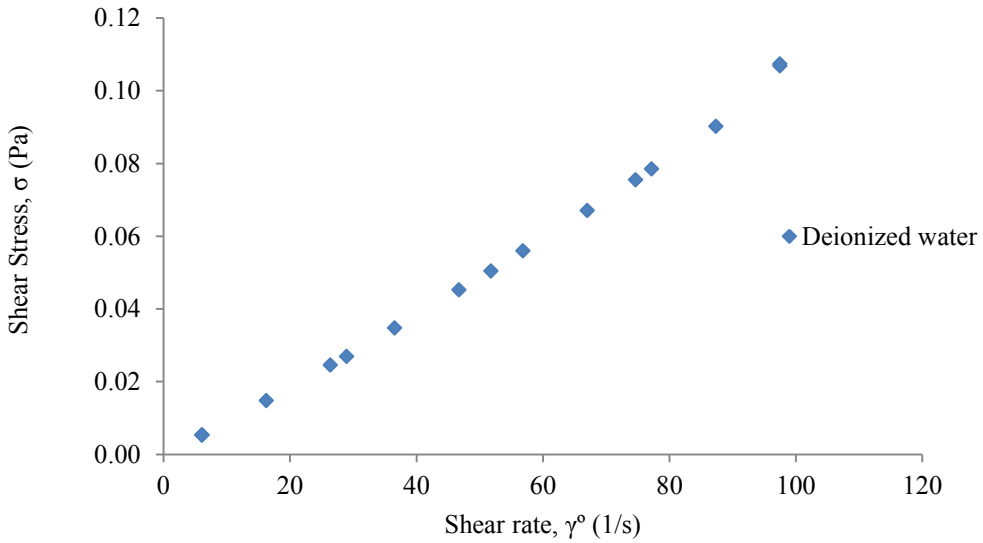

Figure 3-2: Calibration curve of deionized water

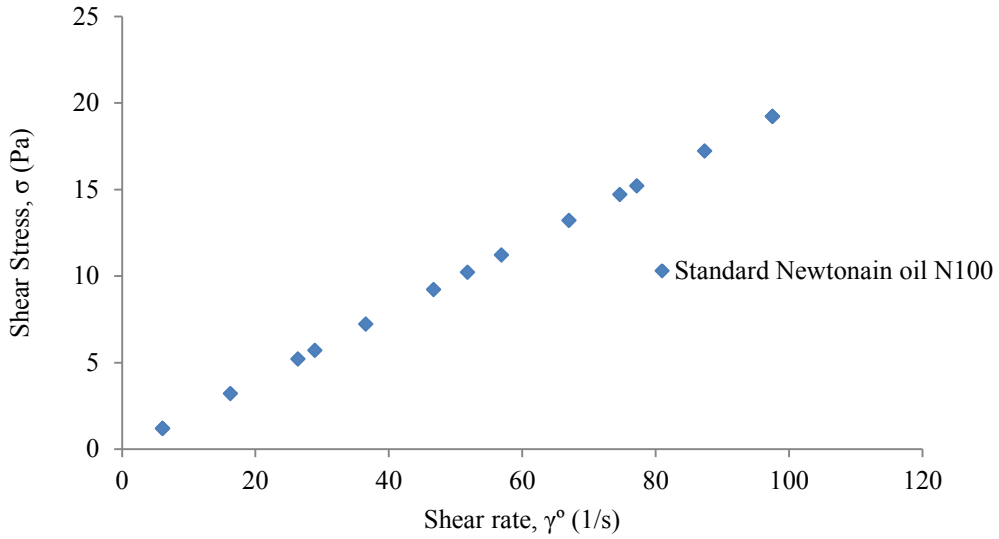

Figure 3-3: Calibration curve of standard Newtonian oil N100

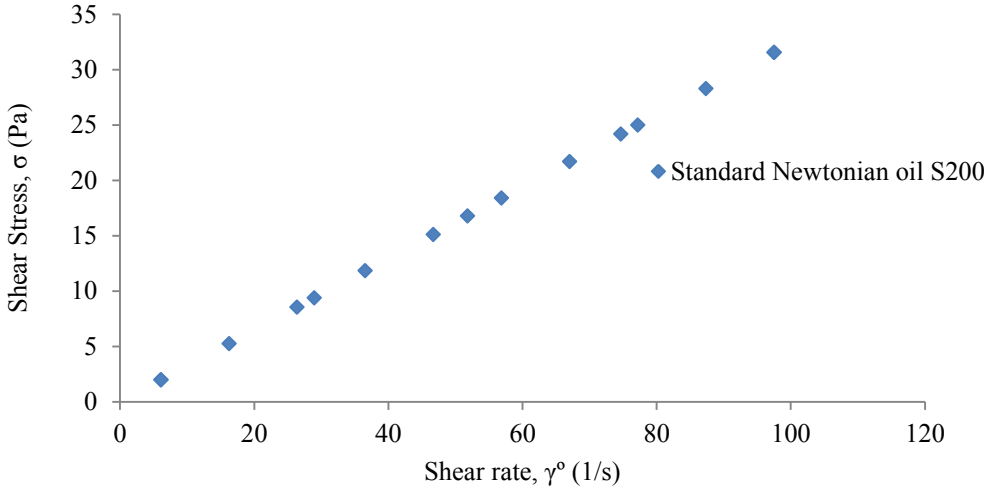

Figure 3-4: Calibration curve of standard Newtonian oil S200

Table 3-2 shows a comparison of the measured viscosities and phase angles and the data provided by the manufacturer.

Table 3-2: Measured and the data provided manufacturer viscosity and phase angles of deionised water and Newtonian standard oils at 25°C

Fluids	Measured μ (Pa·s)	Reported μ (Pa·s)	Measured. Phase angle (º)	Reported. Phase angle (º)
Deionised water	0.000918	0.00890	92.8	90
Oil N100	0.1971	0.2022	90.2	90
Oil S200	0.3237	0.3322	90.1	90

It can be seen that the measured viscosities and phase angles for the deionised water, as well standard oils at the lowest range of torque values (Deionised water) agree with the reported by the manufacturer data within average error of 3.11%.

3.2 Flow through randomly packed column

3.2.1 Experimental setup

As it was indicated earlier, rheological properties of heptane-diluted bitumen solutions in the presence of asphaltene precipitates will also be examined using the flow through porous media.

A flow-loop is shown in Figure 3-5. The circulation loop consists of a peristaltic pump (FH100D), a Rosemount differential pressure cell (DP/Cell), Opto-22 and the Lab-View program running on PC. Peristaltic pump is used to circulate the solution between packed column and 4 liter solution holding tank. The column

was constructed from 0.0253 m inside diameter QV glass pipe. The column is packed with 1 mm uniform size solid glass particles obtained Fischer Scientific. The total packed bed length is 0.593 m. Pressure taps are located at the central of the column and they are 0.293 m apart. The extra 0.15 m extra length packing incorporated on either end of the pressure taps to avoid end effects on pressure drop measurements. The extra length at the inlet end of the column is also used to ensure that the flow is well distributed before the first pressure tap. The DP/cell is used to measure the pressure drops for various solution flow rates. Opto-22 combined with Lab-View program running on PC is used to display and records the pressure drop as a function of time.

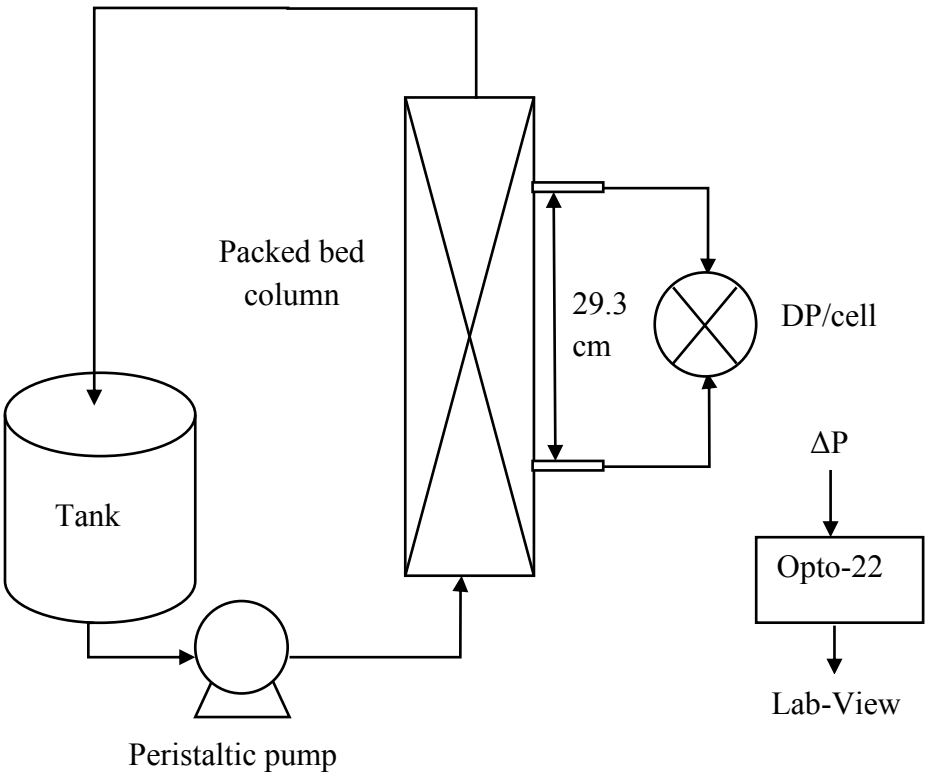

Figure 3-5: A schematic of randomly packed bed column set up

3.2.2 Experimental procedure

Several tests were conducted to determine the accuracy of the experimental data. For these runs, the pressure drops across the packed bed were measured for various n-heptane flow rates as a function of time. During each run, n-heptane volumetric flow rates were determined by timing the volume using stopwatch and graduated cylinder. The mass of the fluid in the graduated cylinder and the temperature were also recorded. The flow rate for each test was measured at least three times to ensure that n-heptane flow rate remained constant during each test. Figure 3-6 shows a comparison between the experimentally determined and predicted friction factors as a function of Reynolds number. The experimental and predicted friction factors were determined using equations (2-14) and (2-15), respectively. The Reynolds number was obtained using equation (2-16). It can be seen that the predicted values obtain using Ergun (1952) [48] equation agree well with the experimental data in the Reynolds number range of 2 and 22. This Figure 3-6 confirms that our experimental data (i.e. pressure drop) are reasonably accurate.

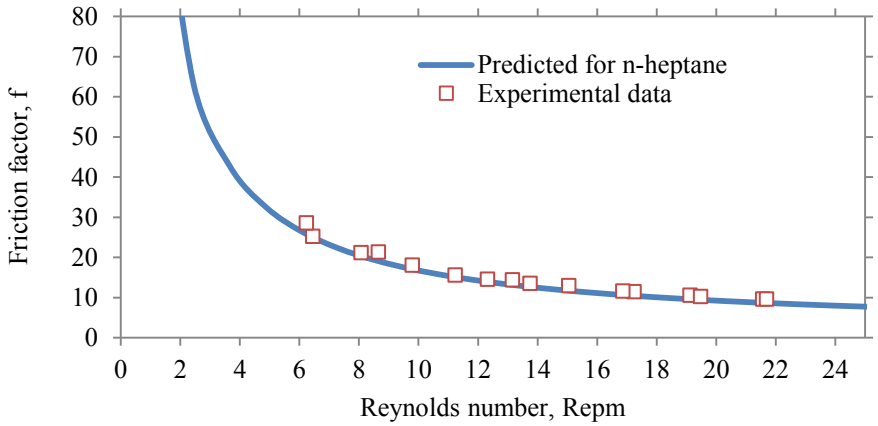

Figure 3-6: Friction factor- Reynolds number relationship for n-heptane.

4 Chapter 4: Results and Discussion

Assessing the solubility of bitumen in n-heptane, ratios of 1:5, 1:10, 1:20, 1:40, 1:60, 1:80, 1:200 wt. % were prepared and solubility of bitumen in n-heptane in different weight fractions were measured. The weight percentage of the solids for each sample, which were not dissolved in n-heptane, is shown in Figure 4-1.

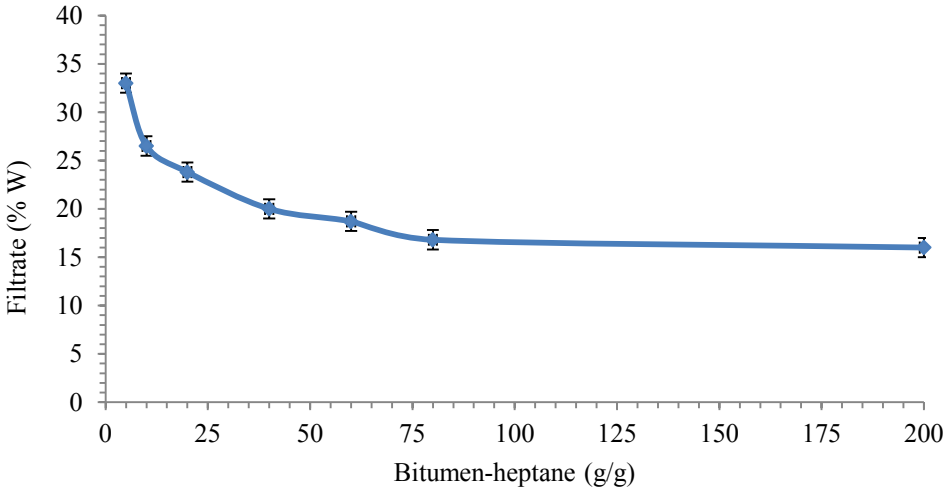

Figure 4-1: Effect of heptane-to-bitumen ratio on the filtrate yield from Athabasca bitumen.

From above figure, it can be seen that the filtrates yield amount from Athabasca bitumen is strong function of n-heptane-to-bitumen ratio. In another word, the solids were not passed through the filter paper decreases with increase the amount of n-heptane in the solution. Also, based on the experimental observation, it seems there are some materials which were trapped through filter paper.

For showing the relationship between the amount of Athabasca asphaltene precipitated and the concentration of n-heptane, Alboudwarej et al. [18] filtered the precipitated asphaltenes from the solvent-crude oil mixture. Then, the filter

cake was washed with solvent to remove trapped materials, and then the asphaltenes were dried and recovered. They demonstrated that washing likely removes trapped maltenens. They expressed that asphaltenes precipitated collected on a filter paper and they formed a layer through which the supernatant drains. So, some maltenes may become trapped within the structure of the precipitate and some maltene components such as resins may adsorb on the asphaltene precipitate. They also found that as n-heptane to bitumen reaches 40:1 cm^3/g, maximum amount of asphaltene precipitate.

The Figure 4-2 shows the relationship between the amount of maltene and asphaltene precipitates as a function of the concentration of n-heptane. It presents the amount of asphaltene precipitates from Alboudwarej et al. [18] (curve b) versus the amount of maltenes, which is calculated by subtracting the amount of asphaltene from filtrate (curve a) that obtain from this study. The amount of maltenes decreases by asphaltene. In other word, in low heptane concentrations maltene is dominating in the filtrate but as the concentration of heptane increases, more asphaltene precipitates form and makes asphaltene dominant at higher heptane concentrations. This alteration in the ratio of asphaltene to maltene is expected to change the behaviour of the filtrate and as a result varies the behaviour of solution.

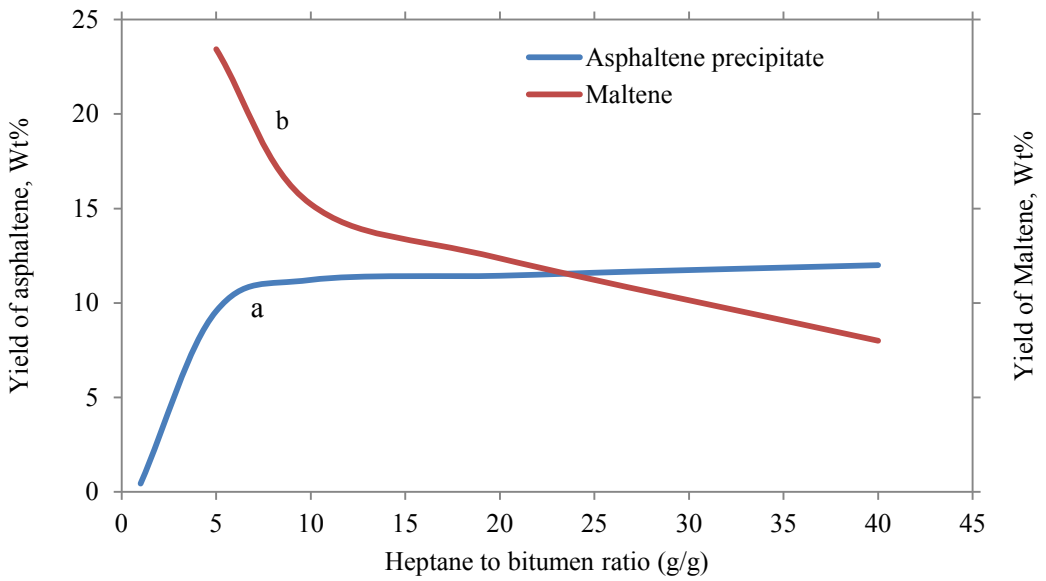

Figure 4-2: a: Relation between the amount of Athabasca asphaltene precipitates and the concentration of n-heptane on the left Y axis [13], b: and relation between the amount maltene and the concentration of n-heptane on the right Y axis.

4.1 Rheological characterization of bitumen-heptane solutions

The viscosity, and phase angle of bitumen--heptane solutions at weight fraction of 1:1, 1:5, 1:10, 1:20, 1:40, 1:60, 1:80, and 1:200 were determined using a AR-G2 rheometer. All measurements were conducted, at 25°C under rotational mapping mode with angular velocity range of 0.5 to 2 rad/s to keep the flow in laminar regime. Furthermore, for all measurement, the oscillation mapping mode was kept constant at amplitude of 0.05 Hz frequency, and 1.5 rad displacement to apply sinusoidal, oscillatory stresses and strains to a thin disc of bitumen, which was sandwiched between the two concentric cylinders to determine the dynamic rheological properties of the bitumen. Figure 4-3 and Figure 4-4 show the viscosity of the solutions and phase angle as a function of various bitumen-

heptane weight fraction solutions, respectively. As it was expected, Figure 4-3 shows that as solvent amount increases the viscosity of the solution decreases.

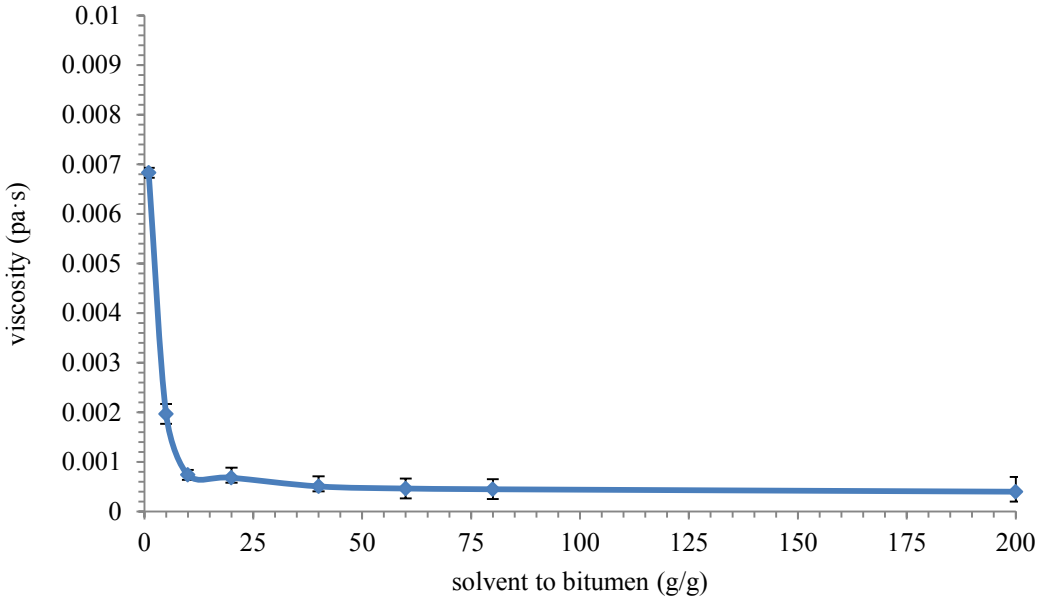

Figure 4-3: Effect of heptane-to-bitumen ratio on the viscosity.

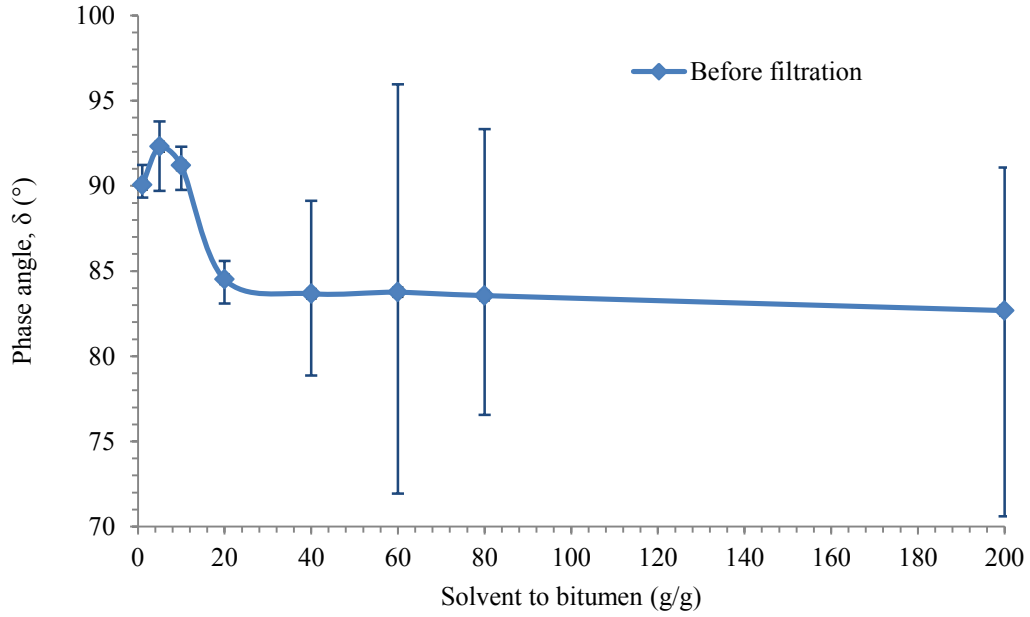

Figure 4-4: Effect of heptane-to-bitumen ratio on the phase angle.

As it was mentioned earlier, the phase angle (δ) is defined as the phase difference between stress and strain, which for purely elastic materials it would be 0°, whereas for purely viscous materials, the phase angle will be 90°; therefore, it would be describing the visco-elastic properties of a material. The results in Figure 4-4 show that for bitumen-heptane solutions at weight fraction of 1:1, 1:5, and 1:10, the phase angle is around 90° out of phase and the solutions are purely viscous. However, for bitumen-heptane solutions at weight fraction of 1:20, 1:40, 1:60, 1:80 and 1:200, the phase angle is around 83° out of phase.

It was mentioned earlier that Alboudwarej et al. [18] found that as n-heptane to bitumen reaches 40:1 cm^3/g, maximum amount of asphaltene precipitate, so it is conjecture that the low phase angle for bitumen-heptane solutions at weight fraction of 1:40, 1:60, 1:80 and 1:200 might be because of the presence of asphaltene in the solutions. So, the solutions were filtered in order to eliminate asphaltene precipitates. Then the rheology of these solutions in the absence of asphaltenes was investigated. Figure 4-5 shows effect of heptane-to-bitumen ratio on the phase angle in the absence of asphaltene for ratios 1:40, 1:60, 1:80, and 1:200.

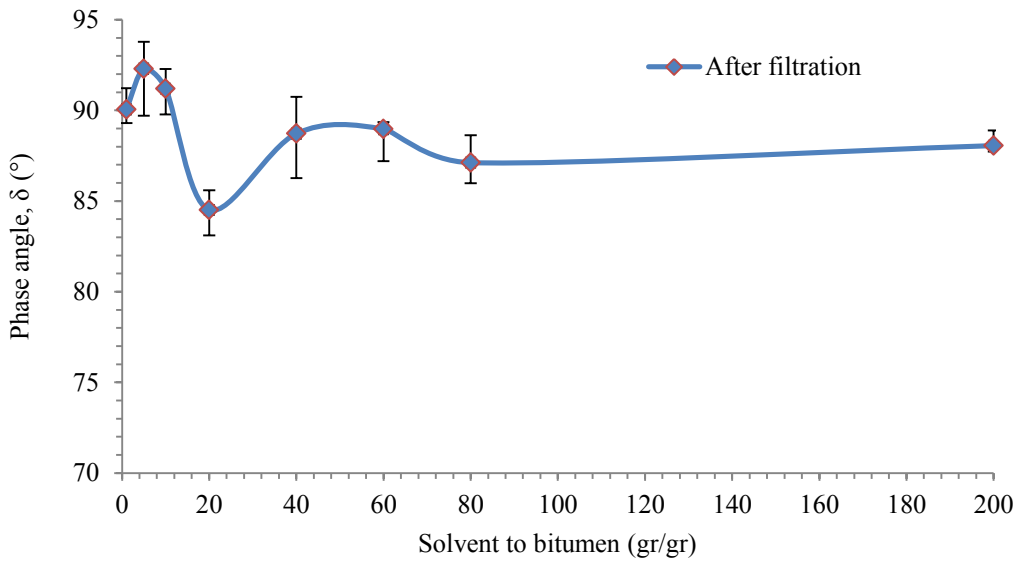

Figure 4-5: Effect of heptane-to-bitumen ratio on the phase angle in the absence of asphaltene for ratios 1:40, 1:60, 1:80, and 1:200.

Interestingly, as it was expected, for bitumen-heptane solutions at weight fraction of 1:40, 1:60, 1:80 and 1:200 the phase angle is 90° out of phase and these solutions in the absence of asphaltene precipitates behave as a Newtonian fluid.

Figure 4-6 shows relation of viscosity to the phase angle of diluted Athabasca bitumen in n-heptane.

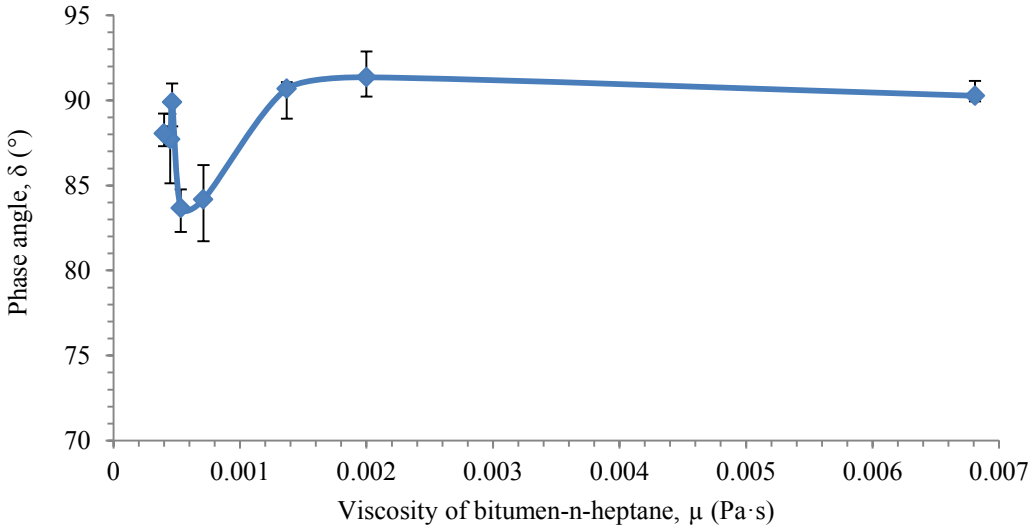

Figure 4-6: Relation of viscosity to the phase angle of diluted Athabasca bitumen in n-heptane.

Figure 4-6 indicates for solutions having the viscosity both around 0.0005 Pa·s and lower, and around 0.001 Pa·s and higher, the phase angle is 90° out of phase and the solutions are purely viscous; while, for solution having viscosity around 0.0007 Pa·s, the phase angle is around 84° out of phase, which means the stress-strain behaviours of these materials are characterized by their elastic and viscous moduli and solution at this concentrate behave as a non-Newtonian liquid.

The rheological behaviour of diluted bitumen in n-heptane in the presence of asphaltene is investigated using flow through porous media to confirm this rheological behaviour.

4.2 Rheological behaviour of n-heptane-bitumen solutions in randomly packed bed column

The rheological behaviour of diluted bitumen in n-heptane in the presence of asphaltene is investigated using flow through porous media. Bitumen-heptane solutions with different concentrations were prepared and were mixed 1 hour, 2 hours and 24 hours. The solution is distributed as uniformly as possible at the bottom of the column and flows upward, wetting the packing material. Then the pressure drops were measured as a function of various solution flow rates Figure 4-7, Figure 4-8, and Figure 4-9 show the predicted and experimentally determined friction factors as a function particle Reynolds number for all solutions after 1hour, 2 hours and 24 hours mixing periods, respectively.

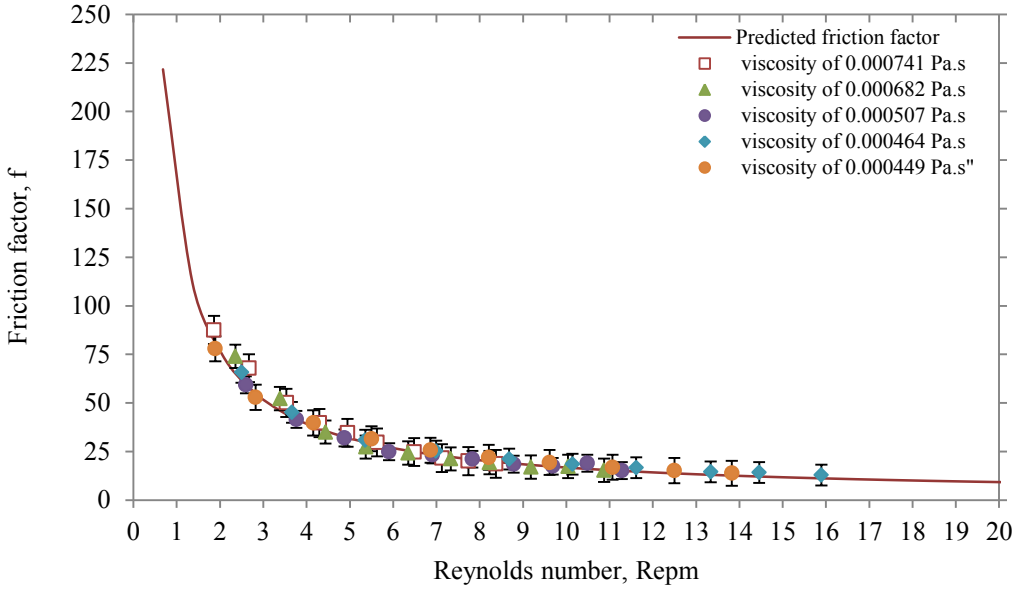

Figure 4-7: Predicted and experimentally determined friction factors as a function of Reynolds number after 1 hour mixing.

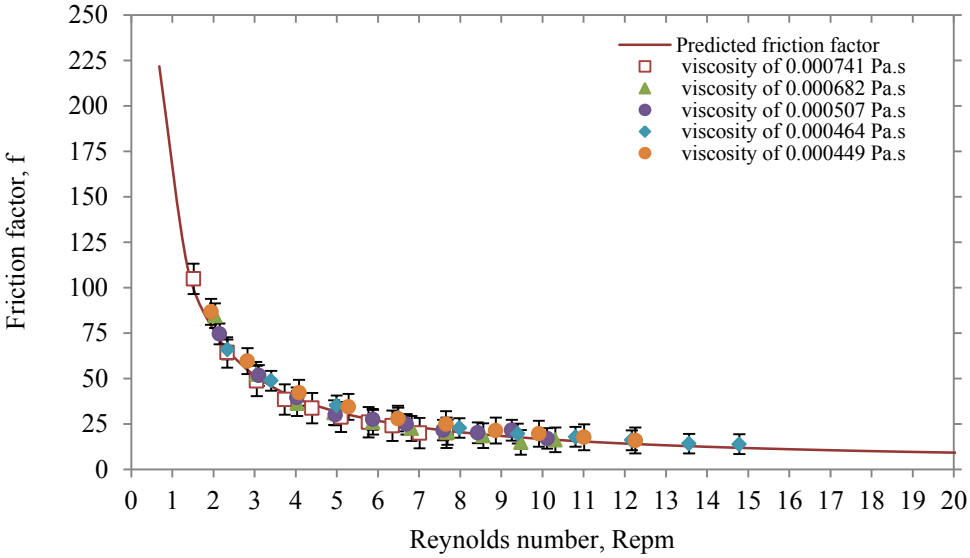

Figure 4-8: Predicted and experimentally determined friction factors as a function of Reynolds number after 2 mixing hours.

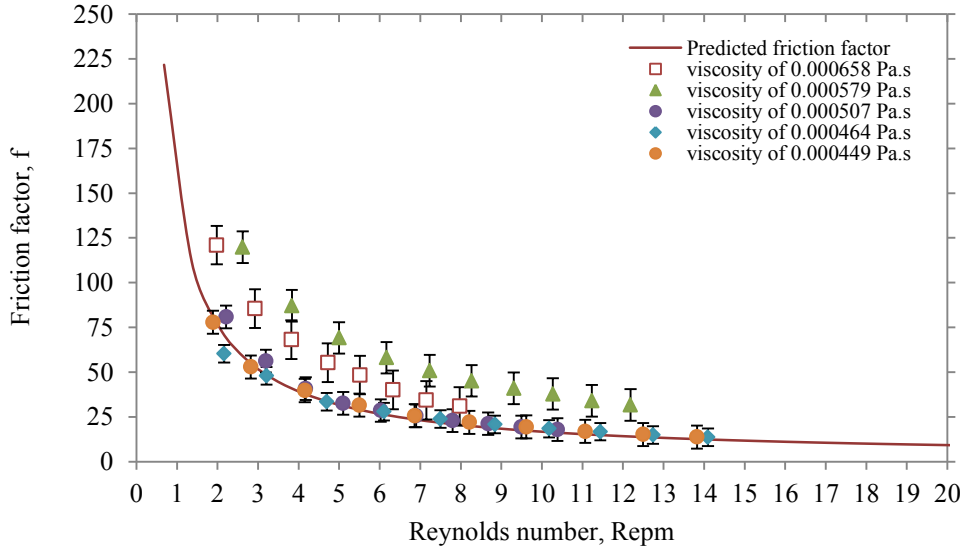

Figure 4-9: Predicted and experimentally determined friction factors as a function unction of Reynolds number after 24 hour mixing.

Figure 4-7 and Figure 4-8 show that for bitumen-heptane solutions after one and two hour mixing, the predicted and the experimentally determined friction factors are in good agreement with each other. Figure 4-9 shows that for bitumen-heptane solutions having viscosity less than 0.0005 Pa·s, the predicted and the experimental friction factors are in good agreement. However, for bitumen-heptane solutions having viscosity around 0.0005 Pa·s to 0.0007 Pa·s, the predicted and experimentally friction factors do not agree with each other.

As indicated earlier, the amount of asphaltenes extracted from a crude oil depends on the type of solvent, dilution ratio, contact time, and temperature. Alboudwarej et al., [18] have demonstrated that the effect of contact time on the amount of precipitated asphaltenes increases over the first few hours reaching an area of stability after approximately 24 hours .We believe that the disagreement shown in Figure 4-10 is due to elevated precipitate asphaltene decrease the void area between the particles after 24 hour mixing. To prove this hypotesis, the packed bed column was washed with toluene to remove all precipitated asphaltenes and then the column was dried with air. The supernatant of the solutions are collected and passed it through the packed bed column. The pressure drops were measured again for various solution flow rates. The comparioson of the predicted and experimentally determined friction factors versus Reynolds number without solids present is shown in Figure 4-10.

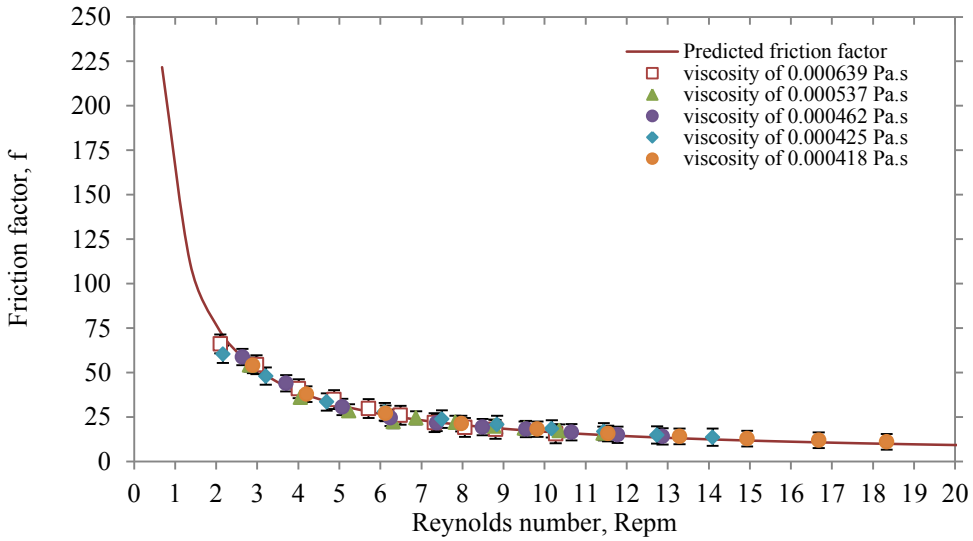

Figure 4-10: Predicted and experimentally determined friction factors as a function of Reynolds number after particulates removed.

It can be seen that for all bitumen-heptane solutions after 24 hour mixing and all precipitated asphaltenes removed, the predicted and experimental friction factors are in good agreement. However, we believe that the disagreement between the experimentall friction factors and the predcited values for the viscosty range between 0.0005 Pa·s and 0.0007 Pa·s shown in Figure 4-9 is not only due to decrease the void area between the particles because of the presence of solids because if that was the only reason for shifting up the measured friction factor compared to the predicted friction factor, the diagram of the measured friction factor for solutions with higher viscosity should have been located above the diagram of solutions with lower viscosity. So, we point out that disagreement for solution having less viscosity (around 0.000537 Pa·s) might be because of the non-Newtonian behaviour of the solution. This result also is in consistence with the results from rheometery meausrment.

Conclusions

Rheological behaviour of bitumen-heptane solution in different concentrations was determined using an AR-G2 rheometer. The results show, when the solutions have the viscosity higher than 0.001 Pa·s and less than 0.0005 Pa·s, the phase angle is around 90° out of phase and the solutions are purely viscous; while for the solutions having the viscosity around 0.0007 ·(ratio 1:20), the phase angle is around 84° out of phase and the solution behave as a Non-Newtonian liquid.

The rheological behaviour of diluted bitumen in n-heptane in the presence of precipitated asphaltenes was also investigated using flow through porous media.

Heptane-bitumen solutions with different concentrations was prepared and passed through randomly packed bed column after 1, 2, and 24 hour after mixing. It was found that for all bitumen-heptane solutions after one and two hours mixing, the predicted and measured friction factors were in good agreement with each other, which indicates that all bitumen-heptane solutions behaves as a Newtonian fluid. However, for bitumen-heptane solution having viscosity around 0.0007 Pa·s (ratio 1:20), after 24 hours mixing of the solutions, the predicted and measured friction factor did not agreed. We believe that this disagreement might be because of both decrease the void area between the particles because of the presence of solids and non- Newtonian behaviour of the solution, which is in consistent with the rheology measurement results. In addition, the results show blockage by particulates in low solvent ratios ($\leq$ 1:20).

Future work

For future work, it is recommended that one study performed to caracterize the filterate to find out the nature of intercation between asphaltene and maltene which could provide better understanding of the mechanism of the non-Newtonian behaviour of the solutions in that area. Also, It would be useful to study the effect of the temperature on the rheological behaviour of heptane-diluted bitumen in the presence of precipitate.

References

[1] Anonymous WORLDWIDE LOOK AT RESERVES AND PRODUCTION. *Oil & Gas Journal* 2012.

[2] Anonymous "Government, Alberta Energy (2014). Oil sands. Alberta, http://www.energy.alberta.ca/oilsands/791.asp,".

[3] J. H. Masliyah, Z. Xu, J. A. Czarnecki and M. Dabros, *Handbook on Theory and Practice of Bitumen Recovery from Athabasca Oil Sands / Jacob H. Masliyah, Jan A. Czarnecki, and Zhenghe Xu.* Cochrane, Alta. : Kingsley Knowledge Pub., c2011-2013, 2011.

[4] T. Maqbool, P. Srikiratiwong and H. S. Fogler. Effect of temperature on the precipitation kinetics of asphaltenes. *Energy and Fuels 25(2),* pp. 694-700. 2011.

[5] Y. Xu, T. Dabros and H. Hamza. Study on the mechanism of foaming from bitumen froth treatment tailings. *Journal of Dispersion Science & Technology 28(3),* pp. 413-418. 2007.

[6] R. B. Dunbar, "Canada's Oil Sands - A World-Scale Hydrocarbon Resource. Strategy West Inc." November 2014.

[7] B. J. Grant, E. Angen and S. Dyer, "Forecasting the impacts of oilsands expansion with each barrel of bitumen production," vol. m, pp. 1-13, 2013.

[8] D. Woynillowicz, C. Severson-Baker and M. Raynolds, "Oil Sands Fever: The Environmental Implications of Canada's Oil Sands Rush. Pembina institute," 2005.

[9] R. M. BUTLER, I. J. MOKRYS and C. UNIV. [R] a new process (vapex) for recovering heavy oils using hot water and hydrocarbon vapour. 1991.

[10] S. K. Das and R. M. Butler. Mechanism of the vapor extraction process for heavy oil and bitumen. *Journal of Petroleum Science and Engineering 21(1-2),* pp. 43-59. 1998.

[11] S. R. Upreti, A. Lohi, R. A. Kapadia and R. El-Haj. Vapor extraction of heavy oil and bitumen: A review. *Energy and Fuels 21(3),* pp. 1562-1574. 2007.

[12] R. M. Butler, I. J. Mokrys and S. K. Das. Solvent requirements for vapex recovery. Presented at Proceedings - SPE International Heavy Oil Symposium. 1995, .

[13] P. Luo, C. Yang, A. K. Tharanivasan and Y. Gu. In situ upgrading of heavy oil in a solvent-based heavy oil recovery process. *J can Pet Technol 46(9),* pp. 37-43. 2007.

[14] L. M. Arciniegas and T. Babadagli. Asphaltene precipitation, flocculation and deposition during solvent injection at elevated temperatures for heavy oil recovery. *Fuel 124*pp. 202-211. 2014.

[15] K. D. Mannistu, H. W. Yarranton and J. H. Masliyah. Solubility modeling of asphaltenes in organic solvents. *Energy and Fuels 11(3),* pp. 615-620. 1997.

[16] G. Hotier and M. Robin. Effects of different thinners on heavy petroleum products: Measuring, interpreting and forecasting asphaltene flocculation. *Rev Inst Fr Pet 38(1),* pp. 101-120. 1983.

[17] I. A. Wiehe, H. W. Yarranton, K. Akbarzadeh, P. M. Rahimi and A. Teclemariam. The paradox of asphaltene precipitation with normal paraffins. *Energy and Fuels 19(4),* pp. 1261-1267. 2005.

[18] H. Alboudwarej, J. Beck, W. Y. Svrcek, H. W. Yarranton and K. Akbarzadeh. Sensitivity of asphaltene properties to separation techniques. *Energy and Fuels 16(2),* pp. 462-469. 2002.

[19] M. R. Gray, *Upgrading of Oil Sands Bitumen and Heavy Oil* . 2010.

[20] S. Badre, C. Carla Goncalves, K. Norinaga, G. Gustavson and O. C. Mullins. Molecular size and weight of asphaltene and asphaltene solubility fractions from coals, crude oils and bitumen. *Fuel 85(1),* pp. 1-11. 2006.

[21] O. León, E. Rogel, J. Espidel and G. Torres. Asphaltenes: Structural characterization, self-association, and stability behavior. *Energy and Fuels 14(1),* pp. 6-10. 2000.

[22] O. P. Strausz, T. W. Mojelsky and E. M. Lown. The molecular structure of asphaltene: An unfolding story. *Fuel 71(12),* pp. 1355-1363. 1992.

[23] O. Sabbagh, K. Akbarzadeh, A. Badamchi-Zadeh, W. Y. Svrcek and H. W. Yarranton. Applying the PR-EoS to asphaltene precipitation from n-alkane diluted heavy oils and bitumens. *Energy and Fuels 20(2),* pp. 625-634. 2006.

[24] S. I. Andersen. Flocculation onset titration of petroleum asphaltenes. *Energy and Fuels 13(2),* pp. 315-322. 1999.

[25] A. Hammami, C. H. Phelps, T. Monger-McClure and T. M. Little. Asphaltene precipitation from live oils: An experimental investigation of onset conditions and reversibility. *Energy and Fuels 14(1),* pp. 14-18. 2000.

[26] A. K. Tharanivasan, W. Y. Svrcek, H. W. Yarranton, S. D. Taylor, D. Merino-Garcia and P. M. Rahimi. Measurement and modeling of asphaltene precipitation from crude oil blends. *Energy and Fuels 23(8),* pp. 3971-3980. 2009.

[27] G. A. Mansoori. Modeling of asphaltene and other heavy organic depositions. *Journal of Petroleum Science and Engineering 17(1-2),* pp. 101-111. 1997.

[28] Y. -. Hu and T. -. Guo. Effect of temperature and molecular weight of n-alkane precipitants on asphaltene precipitation. *Fluid Phase Equilib. 192(1-2),* pp. 13-25. 2001.

[29] S. I. Andersen and K. S. Birdi. Influence of temperature and solvent on the precipitation of asphaltenes. *Fuel Sci. Technol. Int. 8(6),* pp. 593-615. 1990.

[30] S. I. Andersen. Effect of precipitation temperature on the composition of n-heptane asphaltenes. *Fuel Sci. Technol. Int. 12(1),* pp. 51-74. 1994.

[31] H. W. Yarranton and J. H. Masliyah. Molar mass distribution and solubility modeling of asphaltenes. *AICHE J. 42(12),* pp. 3533-3543. 1996.

[32] A. Hirschberg, L. N. J. deJong, B. A. Schipper and J. G. Meijer. Influence of temperature and pressure on asphaltene flocculation. *Society of Petroleum Engineers Journal 24(3),* pp. 283-293. 1984.

[33] H. Lian, J. -. Lin and T. F. Yen. Peptization studies of asphaltene and solubility parameter spectra. *Fuel 73(3),* pp. 423-428. 1994.

[34] M. A. Hasan, M. Fulem, A. Bazyleva and J. M. Shaw. Rheological properties of nanofiltered athabasca bitumen and maya crude oil. *Energy and Fuels 23(10),* pp. 5012-5021. 2009.

[35] J. G. Webster, *The Measurement, Instrumentation, and Sensors Handbook [Electronic Resource] / Editor-in-Chief, John G. Webster.* Boca Raton, Fla. : CRC Press published in cooperation with IEEE Press, c1999, 1999.

[36] D. Wallace, D. Henry, A. Miadonye and V. R. Puttagunta. Viscosity and solubility of mixtures of bitumen and solvent. *Fuel Sci. Technol. Int. 14(3),* pp. 465-478. 1996.

[37] K. Moran and A. Yeung. Determining bitumen viscosity through drop shape recovery. *Can. J. Chem. Eng. 82(4),* pp. 813-820. 2004.

[38] E. L. Dukatz and D. A. Anderson. The effect of various fillers on the mechanical behaviour of asphalt and asphalt concrete. *Proceedings of the Association of Asphalt Paving Technologists 49*pp. 530-549. 1980.

[39] S. H. Ward and K. A. Clark, "Determination of the viscosities and specific gravities of the oils in samples of athabaska bituminous sand [electronic resource]," Edmonton, AB : Research Council of Alberta, 1950, Tech. Rep. 57, 1950.

[40] J. M. Dealy, "Rheological Properties of Oil Sand Bitumens," *Canadian Journal of Chemical Engineering, The,* vol. 57, pp. 677-683, 1979.

[41] R. S. Sanders, J. Schaan, R. Hughes and C. Shook. Performance of sand slurry pipelines in the oil sands industry. *Can. J. Chem. Eng. 82(4),* pp. 850-857. 2004.

[42] R. B. Bird, W. E. Stewart and E. N. Lightfoot, *Transport Phenomena.* New York, NY: John Wiley and Sons Inc., 2002.

[43] C. A. Shook, R. G. Gillies and R. S. Sanders, "Pipeline hydrotransport with applications in the oil sands industry," Saskatchewan Research Council, Saskatoon, SK, 2002.

[44] C. A. Shook and M. C. Roco. *Slurry Flow : Principles and Practice / C.A. Shook, M.C. Roco* 1991[Alberta Innovates - Technology Futures - Mill Woods TJ 898 S559 1991].

[45] G. D. Airey and A. E. Hunter. Dynamic mechanical testing of bitumen: Sample preparation methods. *Proceedings of the Institution of Civil Engineers: Transport 156(2),* pp. 85-92. 2003.

[46] M. J. Rhodes, *Introduction to Particle Technology [Electronic Resource] / Martin Rhodes.* Chichester, England ; Hoboken, NJ : Wiley, c2008; 2nd ed, 2008.

[47] M. M. Denn. *Process Fluid Mechanics / Morton M. Denn.* Printric-Hall, New Jersey, 1980.

[48] J. F. Richardson, J. R. Backhurst, J. M. Coulson and J. H. Harker, *Coulson and Richardson's Chemical Engineering. Volume 2, Particle Technology and Separation Processes [Electronic Resource] / J.F. Richardson, J.H. Harker, with J.R. Backhurst.* Oxford ; Boston : Butterworth-Heinemann, 2002; 5th ed, 2002.

[49] R. H. Perry, D. W. Green and J. O. Maloney, *Perry's Chemical Engineers' Handbook.* New York : McGraw-Hill, 1997; 7th ed. / prepared by a staff of specialists under the editorial direction of late editor Robert H. Perry ; editor, Don W. Green ; assistant editor, James O'Hara Maloney, 1997.

Appendix A

- **Packed bed design**

From a fluid mechanical perspective, the most important issue is that of the pressure drop require for the liquid to flow through the packed bed at a specific flow rate. To calculate this quantity, Ergun equation, which is known for flow through a randomly packed bed of spherical particle of diameters 'D_P' is suggested. It also will be applied when the Re_{pm} is in the range of 1 to 1000, and the porosity of the packed bed column between 0.35 to 0.42.

Ergun equation additively combines the laminar and turbulent components of the pressure gradient. Under laminar condition, the first term dominates and the equation reduced to Carman-Kozeny equation but with the constant 150 rather than 180 which is probably due to the diffrences in shape and packing of the particles. In laminar flow, pressure gradient increase linearly with superficial fluid velocity and independent of fluid density. Under turbulent flow condition, the second term dominates and the equation reduced to Burke-Plummer equation. In this flow, pressure gradient increase as the square of superficial fluid velocity and is independent of fluid viscosity.

Ergun equation: $-\frac{\Delta P}{L} = 150\frac{\mu_f V_s}{D_p^2}\frac{(1-\varepsilon)^2}{\varepsilon^3} + 1.75\left(\frac{(1-\varepsilon)}{\varepsilon^3}\right)\frac{\rho_f V_s^2}{D_p}$

For $Re_{pm} \leq 10$, the C-K equation applies

$$-\frac{\Delta P}{L} = \frac{180\mu_f V_s}{D_p^2}\frac{(1-\varepsilon)^2}{\varepsilon^3}$$

For $Re_{pm} \geq 1000$, the B-P equation applies

$$-\frac{\Delta P}{L} = 1.75 \left(\frac{(1-\varepsilon)}{\varepsilon^3}\right) \frac{\rho_f V_s^2}{D_p}$$

The various symbols appearing in the above equations are defined as follows.

Δp: Pressure Drop

L: Length of the Bed

D_p: Equivalent spherical diameter of the particle defined by $D_p = 6 \frac{\text{Volume of the particle}}{\text{Surface area of the particle}}$

ρ: Density of the fluid

μ: Dynamic viscosity of the fluid

Vs: Superficial velocity (Vs=$\frac{Q}{A}$ where Q is the volumetric flow rate of the fluid and A is the cross-sectional area of the bed)

ε: Void fraction of the bed (ε is the ratio of the void volume to the total volume of the bed) [46, 48, 49].

- **Calculation**

To keep the flow in laminar regime, the Re_{pm} should be ≤10. By assuming Re_{pm}=10, ε =0.35, diameter of the bed=1in, diameter of the glass beads=1mm, and using $Re_{pm} = \frac{D_p V_s \rho}{(1-\varepsilon)\mu}$, the volume flow rate is calculated. Next, the Ergun equation is applied for measuring $\frac{\Delta P}{L}$. In order to find a reasonable L which makes delta P in the measurement capability of the pressure transducer, by try and error L=30 cm is choosen.

The flow capacity of the peristaltic pump is 0.5 to 3000 ml/min; also, the measuring capability of the pressure transducer is up 845 kPa.

The calculation results are shown in the following table.

Table A1: Calculation of pressure drop based on the Ergun equation.

Bitumen heptane (g/g)	**Density of mixture (kg/m^3)**	**Viscosity of mixture (Pa·s)**	**Volume flow rate (mL/min)**	**$\frac{\Delta P}{L}$ (kPa/m)**	**ΔP for L=30cm (kPa)**
1:1	815.35	0.00683	1655.4	613.83	184.15
1:5	722.52	0.00196	536.1	57.04	17.11
1:10	715.01	0.000742	205.1	8.26	2.48
1:20	704.29	0.000682	191.4	7.09	2.13
1:40	689.60	0.000507	145.3	4.00	1.20
1:60	687.24	0.000464	133.4	3.36	1.01
1:80	686.34	0.000449	129.3	3.15	0.95
1:200	684.70	0.0004	115.4	2.51	0.75

Based on the calculations, with having mono-sized glass beads with the diameter of 1mm, and a packed bed in 30 cm length and 1 inch diameter, if the volume flow rate changes from 0 to 100 mL/min, the regime would be laminar ($Re<10$), and the pressure drop would be in the range of the pressure transducer for all samples.

Appendix B

- **Viscosity and phase angle measurement**

Table B1: viscosity and phase angle measurement of n-heptane.

number	Frequency (Hz)	Viscosity (Pa·s)	Phase angle (°)
1	0.05	4.25E-04	93.26
2	0.05	4.06E-04	90.97

Table B2: viscosity and phase angle measurement of bitumen: heptane in the ratio of 1:1 (g/g).

number	Viscosity (Pa·s)	Phase angle (˚)
1	6.81E-03	89.31
2	6.89E-03	91.22
3	6.74E-03	89.53
4	6.91E-03	90.20

Table B3: viscosity and phase angle measurement of bitumen: heptane in the ratio of 1:5 (g/g).

number	Viscosity (Pa·s)	Phase angle (˚)
1	2.00E-03	93.79
2	2.00E-03	93.71
3	1.96E-03	92.00
4	1.91E-03	89.70

Table B4: viscosity and phase angle measurement of bitumen: heptane in the ratio of 1:10 (g/g).

number	Viscosity (Pa·s)	Phase angle (˚)
1	7.55E-04	91.65
2	7.61E-04	92.29
3	7.29E-04	91.09
4	7.26E-04	89.77

Table B5: viscosity and phase angle measurement of bitumen: heptane in the ratio of 1:20 (g/g).

number	Viscosity (Pa·s)	Phase angle (˚)
1	7.11E-04	85.61
2	6.73E-04	83.10
3	6.86E-04	84.88
4	6.60E-04	84.48

Table B6: viscosity and phase angle measurement of bitumen: heptane in the ratio of 1:40 (g/g).

number	Viscosity (Pa·s)	Phase angle (˚)
1	5.32E-04	78.22
2	5.26E-04	83.15
3	4.86E-04	87.02
4	4.84E-04	80.75

Table B7: viscosity and phase angle measurement of bitumen: heptane in the ratio of 1:60 (g/g).

number	Viscosity (Pa·s)	Phase angle (˚)
1	4.64E-04	69.38
2	4.44E-04	75.04
3	4.18E-04	86.90
4	4.52E-04	93.40

Table B8: viscosity and phase angle measurement of bitumen: heptane in the ratio of 1:80 (g/g).

number	Viscosity (Pa·s)	Phase angle (˚)
1	4.49E-04	74.61
2	4.32E-04	81.67
3	4.58E-04	91.39
4	4.60E-04	78.81

Table B9: viscosity and phase angle measurement of bitumen: heptane in the ratio of 1:200 (g/g).

number	Viscosity (Pa·s)	Phase angle (˚)
1	4.00E-04	83.21
2	3.96E-04	91.08
3	3.95E-04	85.83
4	4.20E-04	70.61

Table B10: viscosity and phase angle measurement of bitumen: heptane in the ratio of 1:40 (g/g) without particulates.

number	Viscosity (Pa·s)	Phase angle (°)
1	4.62E-04	88.86
2	4.56E-04	86.27
3	4.48E-04	87.00
4	4.48E-04	92.75

Table B11: viscosity and phase angle measurement of bitumen: heptane in the ratio of 1:60 (g/g) without particulates.

number	Viscosity (Pa·s)	Phase angle (°)
1	4.25E-04	88.36
2	4.26E-04	88.20
3	4.26E-04	87.20
4	4.25E-04	88.13

Table B12: viscosity and phase angle measurement of bitumen: heptane in the ratio of 1:80 (g/g) without particulates.

number	Viscosity (Pa·s)	Phase angle (°)
1	4.17E-04	88.65
2	4.19E-04	87.81
3	4.19E-04	85.98
4	4.17E-04	86.05

Table B13: viscosity and phase angle measurement of bitumen: heptane in the ratio of 1:200 (g/g) without particulates.

number	Viscosity (Pa·s)	Phase angle (°)
1	4.00E-04	88.93
2	3.96E-04	88.77
3	3.95E-04	86.79
4	4.03E-04	87.74

- **Predicted and mesured friction factor**

Re number is calculated by equation (2-16); also, measured and predicted friction factor is calculated by equations (2-14) and (2-16) respectively for all bitumen-heptane solutions.

Predicted and measued friction factor for ratio 1:10 after one hour mixing.

Where ρ_{mix}= 715.01 kg/m^3, μ_{mix}= 0.000742 Pa·s at T=20 °C

Table B14: Predicted friction factor

Re	Predicted *f*
0.68	221.70
1.36	111.72
2.05	75.07
2.73	56.74
3.41	45.74
4.09	38.41
4.77	33.17
5.46	29.24
6.14	26.19
6.82	23.74
7.50	21.75
8.18	20.08
8.87	18.67
9.55	17.46
10.23	16.41
10.91	15.50

Table B15: Measured friction factor

Re	Measured *f*
1.86	87.51
2.67	67.88
3.53	50.05
4.30	39.69
4.95	34.60
5.63	29.69
6.49	24.73
7.13	21.61
7.74	20.06
8.37	18.65

Predicted and measued friction factor for ratio 1:10 after two hours mixing.

Where ρ_{mix}= 715.01 kg/m^3, μ_{mix}= 0.000742 Pa·s at T=20 °C

Table B16: Predicted friction factor

Re	Predicted *f*
0.68	221.70
1.36	111.72
2.05	75.07
2.73	56.74
3.41	45.74
4.09	38.41
4.77	33.17
5.46	29.24
6.14	26.19
6.82	23.74
7.50	21.75
8.18	20.08
8.87	18.67
9.55	17.46
10.23	16.41
10.91	15.50

Table B17: Measured friction factor

Re	Measured *f*
1.52	104.82
2.33	64.32
3.05	48.66
3.73	38.52
4.40	33.74
5.10	28.87
5.77	26.02
6.35	24.00
7.01	20.04
7.67	20.13

Predicted and measued friction factor for ratio 1:10 after 24 hours mixing.

Where ρ_{mix}= 715.01 kg/m^3, μ_{mix}= 0.000658 Pa·s at T=20 °C

Table B18: Predicted friction factor

Re	Predicted *f*
0.68	221.70
1.36	111.72
2.05	75.07
2.73	56.74
3.41	45.74
4.09	38.41
4.77	33.17
5.46	29.24
6.14	26.19
6.82	23.74
7.50	21.75
8.18	20.08
8.87	18.67
9.55	17.46
10.23	16.41
10.91	15.50

Table B19: Measured friction factor

Re	Measured *f*
1.98	120.93
2.92	85.48
3.82	68.14
4.72	55.28
5.51	48.36
6.33	40.10
7.15	34.28
7.97	30.91
8.75	37.14
9.57	36.24

Predicted and measued friction factor for ratio 1:10 after 24 hours mixing without particulates.

Where ρ_{mix}= 715.01 kg/m^3, μ_{mix}= 0.000639 Pa·s at T=20 °C

Table B20: Predicted friction factor

Re	Predicted *f*
0.68	221.70
1.36	111.72
2.05	75.07
2.73	56.74
3.41	45.74
4.09	38.41
4.77	33.17
5.46	29.24
6.14	26.19
6.82	23.74
7.50	21.75
8.18	20.08
8.87	18.67
9.55	17.46
10.23	16.41
10.91	15.50

Table B21: Measured friction factor

Re	Measured *f*
2.10	66.16
2.98	54.48
4.01	40.95
4.87	34.87
5.71	29.81
6.49	25.91
7.32	21.85
8.06	19.22
8.80	18.04
10.27	15.61

Predicted and measued friction factor for ratio 1:20 after one hour mixing.

Where ρ_{mix}= 704.29 kg/m^3, μ_{mix}= 0.000682 Pa·s at T=20 °C

Table B22: Predicted friction factor

Re	Predicted *f*
0.74	203.91
1.48	102.83
2.23	69.14
2.97	52.29
3.71	42.18
4.45	35.44
5.19	30.63
5.94	27.02
6.68	24.21
7.42	21.97
8.16	20.13
8.90	18.60
9.65	17.30
10.39	16.19
11.13	15.23
11.87	14.39
12.61	13.64

Table B23: Measured friction factor

Re	Measured *f*
2.35	73.99
3.39	52.24
4.44	35.01
5.37	27.29
6.35	24.20
7.33	21.20
8.23	19.28
9.18	17.03
10.04	17.26
10.87	15.35

Predicted and measued friction factor for ratio 1:20 after two hours mixing.

Where ρ_{mix}= 704.29 kg/m^3, μ_{mix}= 0.000682 Pa·s at T=20 °C

Table B24: Predicted friction factor

Re	Predicted *f*
0.74	203.91
1.48	102.83
2.23	69.14
2.97	52.29
3.71	42.18
4.45	35.44
5.19	30.63
5.94	27.02
6.68	24.21
7.42	21.97
8.16	20.13
8.90	18.60
9.65	17.30
10.39	16.19
11.13	15.23
11.87	14.39
12.61	13.64

Table B25: Measured friction factor

Re	Measured *f*
2.04	84.54
3.04	52.36
4.03	36.28
4.93	31.20
5.88	25.94
6.82	22.54
7.69	20.46
8.56	18.61
9.47	14.88
10.31	16.26

Predicted and measued friction factor for ratio 1:20 after 24 hours mixing.

Where ρ_{mix}= 704.29 kg/m^3, μ_{mix}= 0.000579 Pa·s at T=20 °C

Table B26: Predicted friction factor

Re	Predicted *f*
0.74	203.91
1.48	102.83
2.23	69.14
2.97	52.29
3.71	42.18
4.45	35.44
5.19	30.63
5.94	27.02
6.68	24.21
7.42	21.97
8.16	20.13
8.90	18.60
9.65	17.30
10.39	16.19
11.13	15.23
11.87	14.39
12.61	13.64

Table B27: Measured friction factor

Re	Measured *f*
2.62	119.86
3.83	87.08
5.00	69.15
6.17	58.09
7.23	50.80
8.27	45.16
9.31	40.96
10.27	37.84
11.23	33.99
12.19	31.71

Predicted and measued friction factor for ratio 1:20 after 24 hours mixing without particulates.

Where ρ_{mix}= 704.29 kg/m^3, μ_{mix}= 0.000537 Pa·s at T=20 °C

Table B28: Predicted friction factor

Re	Predicted *f*
0.74	203.91
1.48	102.83
2.23	69.14
2.97	52.29
3.71	42.18
4.45	35.44
5.19	30.63
5.94	27.02
6.68	24.21
7.42	21.97
8.16	20.13
8.90	18.60
9.65	17.30
10.39	16.19
11.13	15.23
11.87	14.39
12.61	13.64

Table B29: Measured friction factor

Re	Measured *f*
2.81	54.14
4.05	36.11
5.23	28.56
6.32	22.35
6.87	24.55
7.82	22.11
8.77	19.93
9.51	18.78
10.36	17.29
11.43	15.87

Predicted and measued friction factor for ratio 1:40 after one hour mixing.

Where ρ_{mix}= 689.6 kg/m^3, μ_{mix}= 0.000507 Pa·s at T=20 °C

Table B30: Predicted friction factor

Re	Predicted *f*
1.00	152.04
2.00	76.89
2.99	51.85
3.99	39.32
4.99	31.81
5.99	26.80
6.99	23.22
7.98	20.54
8.98	18.45
9.98	16.78
10.98	15.41
11.98	14.27
12.98	13.31

Table B31: Measured friction factor

Re	Measured *f*
2.60	59.37
3.76	41.49
4.87	31.93
5.90	24.86
6.91	23.19
7.83	21.03
8.79	18.52
9.68	17.41
10.49	18.98
11.28	15.24

Predicted and measued friction factor for ratio 1:40 after two hours mixing.

Where ρ_{mix}= 689.6 kg/m^3, μ_{mix}= 0.000507 Pa·s at T=20 °C

Table B32: Predicted friction factor

Re	Predicted *f*
1.00	152.04
2.00	76.89
2.99	51.85
3.99	39.32
4.99	31.81
5.99	26.80
6.99	23.22
7.98	20.54
8.98	18.45
9.98	16.78
10.98	15.41
11.98	14.27
12.98	13.31

Table B33: Measured friction factor

Re	Measured *f*
2.15	74.57
3.10	51.69
4.03	39.45
4.97	30.02
5.87	27.59
6.69	24.83
7.58	21.63
8.42	20.15
9.25	21.61
10.11	17.08

Predicted and measued friction factor for ratio 1:40 after 24 hours mixing.

Where ρ_{mix}= 689.6 kg/m^3, μ_{mix}= 0.000507 Pa·s at T=20 °C

Table B34: Predicted friction factor

Re	Predicted *f*
1.00	152.04
2.00	76.89
2.99	51.85
3.99	39.32
4.99	31.81
5.99	26.80
6.99	23.22
7.98	20.54
8.98	18.45
9.98	16.78
10.98	15.41
11.98	14.27
12.98	13.31

Table B35: Measured friction factor

Re	Measured *f*
2.21	80.84
3.19	56.14
4.18	40.84
5.10	32.52
6.02	28.58
6.90	25.65
7.79	22.90
8.67	21.20
9.49	19.34
10.38	17.93

Predicted and measued friction factor for ratio 1:40 after 24 hours mixing without particulates.

Where ρ_{mix}= 689.6 kg/m^3, μ_{mix}= 0.000462 Pa·s at T=20 °C

Table B36: Predicted friction factor

Re	Predicted *f*
1.00	152.04
2.00	76.89
2.99	51.85
3.99	39.32
4.99	31.81
5.99	26.80
6.99	23.22
7.98	20.54
8.98	18.45
9.98	16.78
10.98	15.41
11.98	14.27
12.98	13.31

Table B37: Measured friction factor

Re	Measured *f*
2.64	58.67
3.70	43.97
5.08	30.64
6.24	24.47
7.37	21.63
8.49	19.35
9.55	18.24
10.66	16.50
11.78	15.08
12.87	14.02

Predicted and measued friction factor for ratio 1:60 after one hour mixing.

Where ρ_{mix}= 687.24 kg/m^3, μ_{mix}= 0.000464 Pa·s at T=20 °C

Table B38: Predicted friction factor

Re	Predicted *f*
1.09	139.29
2.18	70.52
3.27	47.60
4.36	36.14
5.45	29.26
6.54	24.67
7.63	21.40
8.72	18.94
9.82	17.03
10.91	15.50
12.00	14.25
13.09	13.21
14.18	12.33
15.27	11.57
16.36	10.92

Table B39: Measured friction factor

Re	Measured *f*
2.50	65.75
3.66	45.22
5.36	30.85
6.99	25.29
8.68	21.14
10.14	18.52
11.62	16.64
13.34	14.59
14.46	14.16
15.89	12.88

Predicted and measued friction factor for ratio 1:60 after two hours mixing.

Where ρ_{mix}= 687.24 kg/m^3, μ_{mix}= 0.000464 Pa·s at T=20 °C

Table B40: Predicted friction factor

Re	Predicted *f*
1.09	139.29
2.18	70.52
3.27	47.60
4.36	36.14
5.45	29.26
6.54	24.67
7.63	21.40
8.72	18.94
9.82	17.03
10.91	15.50
12.00	14.25
13.09	13.21
14.18	12.33
15.27	11.57
16.36	10.92

Table B41: Measured friction factor

Re	Measured *f*
2.34	65.98
3.40	48.77
4.99	35.21
6.49	28.46
7.98	22.79
9.40	19.67
10.80	17.95
12.17	16.06
13.56	14.19
14.78	13.88

Predicted and measued friction factor for ratio 1:60 after 24 hours mixing.

Where ρ_{mix}= 687.24 kg/m^3, μ_{mix}= 0.000464 Pa·s at T=20 °C

Table B42: Predicted friction factor

Re	Predicted *f*
1.09	139.29
2.18	70.52
3.27	47.60
4.36	36.14
5.45	29.26
6.54	24.67
7.63	21.40
8.72	18.94
9.82	17.03
10.91	15.50
12.00	14.25
13.09	13.21
14.18	12.33
15.27	11.57
16.36	10.92

Table B43: Measured friction factor

Re	Measured *f*
2.16	60.27
3.21	47.97
4.69	33.49
6.11	27.94
7.50	23.83
8.84	20.76
10.18	18.38
11.44	16.75
12.74	14.88
14.09	13.61

Predicted and measued friction factor for ratio 1:60 after 24 hours mixing without particulates.

Where ρ_{mix}= 687.24 kg/m^3, μ_{mix}= 0.000425 Pa·s at T=20 °C

Table B44: Predicted friction factor

Re	Predicted *f*
1.09	139.29
2.18	70.52
3.27	47.60
4.36	36.14
5.45	29.26
6.54	24.67
7.63	21.40
8.72	18.94
9.82	17.03
10.91	15.50
12.00	14.25
13.09	13.21
14.18	12.33
15.27	11.57
16.36	10.92

Table B45: Measured friction factor

Re	Measured *f*
2.16	60.27
3.21	47.97
4.69	33.49
6.11	27.94
7.50	23.83
8.84	20.76
10.18	18.38
11.44	16.75
12.74	14.88
14.09	13.61

Predicted and measued friction factor for ratio 1:80 after one hour mixing.

Where ρ_{mix}= 686.34 kg/m^3, μ_{mix}= 0.000449 Pa·s at T=20 °C

Table B46: Predicted friction factor

Re	Predicted *f*
1.13	134.84
2.25	68.30
3.38	46.11
4.51	35.02
5.64	28.37
6.76	23.93
7.89	20.76
9.02	18.39
10.14	16.54
11.27	15.06
12.40	13.85
13.52	12.84
14.65	11.99
15.78	11.26
16.91	10.62
18.03	10.07
19.16	9.58

Table B47: Measured friction factor

Re	Measured *f*
1.89	77.86
2.82	52.88
4.15	39.73
5.50	31.54
6.86	25.69
8.21	21.95
9.61	19.36
11.07	16.90
12.50	15.17
13.82	13.78

Predicted and measued friction factor for ratio 1:80 after two hours mixing.

Where ρ_{mix}= 686.34 kg/m^3, μ_{mix}= 0.000449 Pa·s at T=20 °C

Table B48: Predicted friction factor

Re	Predicted *f*
1.13	134.84
2.25	68.30
3.38	46.11
4.51	35.02
5.64	28.37
6.76	23.93
7.89	20.76
9.02	18.39
10.14	16.54
11.27	15.06
12.40	13.85
13.52	12.84
14.65	11.99
15.78	11.26
16.91	10.62
18.03	10.07
19.16	9.58

Table B49: Measured friction factor

Re	Measured *f*
1.94	86.65
2.82	59.57
4.08	42.12
5.28	34.38
6.48	27.99
7.65	24.96
8.86	21.37
9.91	19.68
11.01	17.63
12.26	15.88

Predicted and measued friction factor for ratio 1:80 after 24 hours mixing.

Where ρ_{mix}= 686.34 kg/m^3, μ_{mix}= 0.000449 Pa·s at T=20 °C

Table B50: Predicted friction factor

Re	Predicted *f*
1.13	134.84
2.25	68.30
3.38	46.11
4.51	35.02
5.64	28.37
6.76	23.93
7.89	20.76
9.02	18.39
10.14	16.54
11.27	15.06
12.40	13.85
13.52	12.84
14.65	11.99
15.78	11.26
16.91	10.62
18.03	10.07
19.16	9.58

Table B51: Measured friction factor

Re	Measured *f*
1.89	77.86
2.82	52.88
4.15	39.73
5.50	31.54
6.86	25.69
8.21	21.95
9.61	19.36
11.07	16.90
12.50	15.17
13.82	13.78

Predicted and measued friction factor for ratio 1:80 after 24 hours mixing without particulates.

Where ρ_{mix}= 686.34 kg/m^3, μ_{mix}= 0.000418 Pa·s at T=20 °C

Table B52: Predicted friction factor

Re	Predicted *f*
1.13	134.84
2.25	68.30
3.38	46.11
4.51	35.02
5.64	28.37
6.76	23.93
7.89	20.76
9.02	18.39
10.14	16.54
11.27	15.06
12.40	13.85
13.52	12.84
14.65	11.99
15.78	11.26
16.91	10.62
18.03	10.07
19.16	9.58

Table B53: Measured friction factor

Re	Measured *f*
2.89	54.06
4.20	37.89
6.13	27.06
7.97	21.34
9.82	18.17
11.55	15.75
13.29	14.16
14.93	12.85
16.68	11.89
18.33	11.00

- **Predicted and mesured pressure drop**

Ergun equation is used to determine the predicted pressure drop for all bitumen-heptane ratios.

Predicted and measued pressure drop for ratio 1:10 after one hour mixing.

Table B54: Predicted pressure drop

Fluid velocity (cm/s)	Predicted ΔP (Pa)
0.05	149.01
0.09	300.36
0.14	454.08
0.18	610.14
0.23	768.55
0.28	929.32
0.32	1092.44
0.37	1257.92
0.41	1425.74
0.46	1595.92
0.51	1768.45
0.55	1943.33
0.60	2120.57
0.64	2300.16
0.69	2482.09
0.74	2666.39
0.78	2853.03
0.83	3042.03
0.87	3233.38
0.92	3427.08
0.97	3623.13
1.01	3821.54

Table B55: Measured pressure drop

Fluid velocity (cm/s)	Measured ΔP (Pa)
0.13	437.40
0.18	698.69
0.24	902.45
0.29	1058.63
0.33	1222.53
0.38	1358.78
0.44	1503.00
0.48	1586.45
0.52	1735.65
0.56	1888.84

Predicted and measued pressure drop for ratio 1:10 after two hours mixing.

Table B56: Predicted pressure drop

Fluid velocity (cm/s)	Predicted ΔP (Pa)
0.05	149.01
0.09	300.36
0.14	454.08
0.18	610.14
0.23	768.55
0.28	929.32
0.32	1092.44
0.37	1257.92
0.41	1425.74
0.46	1595.92
0.51	1768.45
0.55	1943.33
0.60	2120.57
0.64	2300.16
0.69	2482.09
0.74	2666.39
0.78	2853.03
0.83	3042.03
0.87	3233.38
0.92	3427.08
0.97	3623.13
1.01	3821.54

Table B57: Measured pressure drop

Fluid velocity (cm/s)	Measured ΔP (Pa)
0.10	348.48
0.16	505.90
0.21	655.10
0.25	775.66
0.30	942.55
0.34	1084.53
0.39	1252.17
0.43	1398.39
0.47	1423.29
0.52	1709.50

Predicted and measued pressure drop for ratio 1:10 after 24 hours mixing.

Table B58: Predicted pressure drop

Fluid velocity (cm/s)	Predicted ΔP (Pa)
0.05	132.27
0.09	266.89
0.14	403.87
0.18	543.20
0.23	684.88
0.28	828.91
0.32	975.30
0.37	1124.03
0.41	1275.12
0.46	1428.57
0.51	1584.36
0.55	1742.51
0.60	1903.01
0.64	2065.86
0.69	2231.06
0.74	2398.62
0.78	2568.53
0.83	2740.79
0.87	2915.40
0.92	3092.37
0.97	3271.69
1.01	3453.36

Table B59: Measured pressure drop

Fluid velocity (cm/s)	Measured ΔP (Pa)
0.17	830.71
0.23	1131.11
0.28	1400.88
0.33	1670.39
0.38	1824.33
0.43	1991.22
0.48	2233.58
0.52	3232.92
0.57	3773.95

Predicted and measued pressure drop for ratio 1:10 after 24 hours mixing without particulates.

Table B60: Predicted pressure drop

Fluid velocity (cm/s)	Predicted ΔP (Pa)
0.05	128.49
0.09	259.32
0.14	392.51
0.18	528.06
0.23	665.95
0.28	806.20
0.32	948.80
0.37	1093.75
0.41	1241.05
0.46	1390.71
0.51	1542.72
0.55	1697.08
0.60	1853.80
0.64	2012.86
0.69	2174.28
0.74	2338.05
0.78	2504.18
0.83	2672.65
0.87	2843.48
0.92	3016.66
0.97	3192.20
1.01	3370.08

Table B61: Measured pressure drop

Fluid velocity (cm/s)	Measured ΔP (Pa)
0.12	312.86
0.17	519.35
0.23	705.17
0.28	887.01
0.33	1042.44
0.38	1168.73
0.43	1253.91
0.47	1337.36
0.51	1498.77
0.60	1764.30

Predicted and measued pressure drop for ratio 1:20 after one hour mixing.

Table B62: Predicted pressure drop

Fluid velocity (cm/s)	Predicted ΔP (Pa)
0.05	139.14
0.09	280.66
0.14	424.58
0.19	570.88
0.23	719.57
0.28	870.65
0.33	1024.12
0.37	1179.98
0.42	1338.22
0.47	1498.85
0.51	1661.87
0.56	1827.28
0.61	1995.08
0.65	2165.26
0.70	2337.84
0.75	2512.80
0.79	2690.15
0.84	2869.89
0.89	3052.01
0.93	3236.53
0.98	3423.43
1.03	3612.72

Table B63: Measured pressure drop

Fluid velocity (cm/s)	Measured ΔP (Pa)
0.15	508.39
0.21	742.28
0.28	854.37
0.34	974.19
0.40	1208.08
0.46	1411.84
0.52	1616.59
0.58	1779.74
0.63	2155.86
0.68	2249.27

Predicted and measued pressure drop for ratio 1:20 after two hours mixing.

Table B64: Predicted pressure drop

Fluid velocity (cm/s)	Predicted ΔP (Pa)
0.05	139.14
0.09	280.66
0.14	424.58
0.19	570.88
0.23	719.57
0.28	870.65
0.33	1024.12
0.37	1179.98
0.42	1338.22
0.47	1498.85
0.51	1661.87
0.56	1827.28
0.61	1995.08
0.65	2165.26
0.70	2337.84
0.75	2512.80
0.79	2690.15
0.84	2869.89
0.89	3052.01
0.93	3236.53
0.98	3423.43
1.03	3612.72

Table B65: Measured pressure drop

Fluid velocity (cm/s)	Measured ΔP (Pa)
0.13	435.41
0.19	599.81
0.25	731.57
0.31	939.81
0.37	1109.94
0.43	1297.75
0.48	1499.52
0.54	1688.82
0.60	1654.95
0.65	2143.16

Predicted and measued pressure drop for ratio 1:20 after 24 hours mixing.

Table B66: Predicted pressure drop

Fluid velocity (cm/s)	Predicted ΔP (Pa)
0.05	118.31
0.09	239.00
0.14	362.08
0.19	487.55
0.23	615.41
0.28	745.65
0.33	878.29
0.37	1013.31
0.42	1150.72
0.47	1290.52
0.51	1432.71
0.56	1577.28
0.61	1724.25
0.65	1873.60
0.70	2025.34
0.75	2179.47
0.79	2335.98
0.84	2494.89
0.89	2656.18
0.93	2819.86
0.98	2985.93
1.03	3154.39

Table B67: Measured pressure drop

Fluid velocity (cm/s)	Measured ΔP (Pa)
0.14	735.56
0.20	1143.57
0.27	1543.11
0.33	1974.53
0.39	2374.56
0.44	2756.42
0.50	3168.91
0.55	3565.46
0.60	3830.49

Predicted and measued pressure drop for ratio 1:20 after 24 hours mixing without particulates.

Table B68: Predicted pressure drop

Fluid velocity (cm/s)	Predicted ΔP (Pa)
0.05	109.81
0.09	222.01
0.14	336.59
0.19	453.57
0.23	572.93
0.28	694.68
0.33	818.82
0.37	945.35
0.42	1074.27
0.47	1205.57
0.51	1339.26
0.56	1475.34
0.61	1613.81
0.65	1754.67
0.70	1897.91
0.75	2043.55
0.79	2191.57
0.84	2341.98
0.89	2494.77
0.93	2649.96
0.98	2807.53
1.03	2967.50

Table B69: Measured pressure drop

Fluid velocity (cm/s)	Measured ΔP (Pa)
0.14	329.54
0.20	455.83
0.26	600.80
0.31	684.99
0.34	890.49
0.39	1039.95
0.43	1177.44
0.47	1305.23
0.51	1425.54
0.57	1591.93

Predicted and measued pressure drop for ratio 1:40 after one hour mixing.

Table B70: Predicted pressure drop

Fluid velocity (cm/s)	Predicted ΔP (Pa)
0.05	105.95
0.10	214.34
0.14	325.17
0.19	438.44
0.24	554.15
0.29	672.30
0.33	792.88
0.38	915.91
0.43	1041.38
0.48	1169.28
0.52	1299.62
0.57	1432.40
0.62	1567.62
0.67	1705.28
0.72	1845.38
0.76	1987.92
0.81	2132.90
0.86	2280.32
0.91	2430.17
0.95	2582.47
1.00	2737.20
1.05	2894.37

Table B71: Measured pressure drop

Fluid velocity (cm/s)	Measured ΔP (Pa)
0.12	280.47
0.18	411.25
0.23	530.81
0.28	606.28
0.33	773.67
0.37	901.95
0.42	999.84
0.46	1142.32
0.50	1459.91
0.54	1357.78

Predicted and measued pressure drop for ratio 1:40 after two hours mixing.

Table B72: Predicted pressure drop

Fluid velocity (cm/s)	Predicted ΔP (Pa)
0.05	105.95
0.10	214.34
0.14	325.17
0.19	438.44
0.24	554.15
0.29	672.30
0.33	792.88
0.38	915.91
0.43	1041.38
0.48	1169.28
0.52	1299.62
0.57	1432.40
0.62	1567.62
0.67	1705.28
0.72	1845.38
0.76	1987.92
0.81	2132.90
0.86	2280.32
0.91	2430.17
0.95	2582.47
1.00	2737.20
1.05	2894.37

Table B73: Measured pressure drop

Fluid velocity (cm/s)	Measured ΔP (Pa)
0.10	240.37
0.15	347.48
0.19	447.11
0.24	517.86
0.28	665.07
0.32	778.15
0.36	869.82
0.40	1000.09
0.44	1294.02
0.48	1221.78

Predicted and measued pressure drop for ratio 1:40 after 24 hours mixing.

Table B74: Predicted pressure drop

Fluid velocity (cm/s)	Predicted ΔP (Pa)
0.05	105.95
0.10	214.34
0.14	325.17
0.19	438.44
0.24	554.15
0.29	672.30
0.33	792.88
0.38	915.91
0.43	1041.38
0.48	1169.28
0.52	1299.62
0.57	1432.40
0.62	1567.62
0.67	1705.28
0.72	1845.38
0.76	1987.92
0.81	2132.90
0.86	2280.32
0.91	2430.17
0.95	2582.47
1.00	2737.20
1.05	2894.37

Table B75: Measured pressure drop

Fluid velocity (cm/s)	Measured ΔP (Pa)
0.11	276.99
0.15	400.29
0.20	498.18
0.24	591.34
0.29	725.60
0.33	853.88
0.37	973.19
0.41	1115.92
0.45	1219.04

Predicted and measued pressure drop for ratio 1:40 after 24 hours mixing without particulates.

Table B76: Predicted pressure drop

Fluid velocity (cm/s)	Predicted ΔP (Pa)
0.05	105.95
0.10	214.34
0.14	325.17
0.19	438.44
0.24	554.15
0.29	672.30
0.33	792.88
0.38	915.91
0.43	1041.38
0.48	1169.28
0.52	1299.62
0.57	1432.40
0.62	1567.62
0.67	1705.28
0.72	1845.38
0.76	1987.92
0.81	2132.90
0.86	2280.32
0.91	2430.17
0.95	2582.47
1.00	2737.20
1.05	2894.37

Table B77: Measured pressure drop

Fluid velocity (cm/s)	Measured ΔP (Pa)
0.11	237.38
0.16	350.47
0.22	458.57
0.27	553.97
0.32	682.75
0.37	810.04
0.42	965.47
0.46	1088.27
0.51	1214.81
0.56	1349.31

Predicted and measued pressure drop for ratio 1:60 after one hour mixing.

Table B78: Predicted pressure drop

Fluid velocity (cm/s)	Predicted ΔP (Pa)
0.05	97.40
0.10	197.25
0.14	299.55
0.19	404.30
0.24	511.49
0.29	621.13
0.34	733.22
0.38	847.75
0.43	964.73
0.48	1084.16
0.53	1206.04
0.57	1330.36
0.62	1457.14
0.67	1586.36
0.72	1718.02
0.77	1852.14
0.81	1988.70
0.86	2127.71
0.91	2269.17
0.96	2413.07
1.01	2559.42
1.05	2708.22

Table B79: Measured pressure drop

Fluid velocity (cm/s)	Measured ΔP (Pa)
0.11	216.21
0.16	331.29
0.24	495.69
0.31	701.93
0.38	911.42
0.45	1045.18
0.51	1245.44
0.59	1450.94
0.63	1665.41
0.70	1838.53

Predicted and measued pressure drop for ratio 1:60 after two hours mixing.

Table B80: Predicted pressure drop

Fluid velocity (cm/s)	Predicted ΔP (Pa)
0.05	97.40
0.10	197.25
0.14	299.55
0.19	404.30
0.24	511.49
0.29	621.13
0.34	733.22
0.38	847.75
0.43	964.73
0.48	1084.16
0.53	1206.04
0.57	1330.36
0.62	1457.14
0.67	1586.36
0.72	1718.02
0.77	1852.14
0.81	1988.70
0.86	2127.71
0.91	2269.17
0.96	2413.07
1.01	2559.42
1.05	2708.22

Table B81: Measured pressure drop

Fluid velocity (cm/s)	Measured ΔP (Pa)
0.10	211.97
0.15	331.79
0.22	515.86
0.28	705.42
0.35	852.88
0.41	996.11
0.47	1206.59
0.53	1373.73
0.60	1509.98
0.65	1759.07

Predicted and measued pressure drop for ratio 1:60 after 24 hours mixing.

Table B82: Predicted pressure drop

Fluid velocity (cm/s)	Predicted ΔP (Pa)
0.05	89.32
0.10	181.08
0.14	275.30
0.19	371.96
0.24	471.07
0.29	572.62
0.34	676.63
0.38	783.08
0.43	891.98
0.48	1003.32
0.53	1117.12
0.57	1233.36
0.62	1352.05
0.67	1473.18
0.72	1596.76
0.77	1722.79
0.81	1851.27
0.86	1982.20
0.91	2115.57
0.96	2251.39
1.01	2389.66
1.05	2530.37

Table B83: Measured pressure drop

Fluid velocity (cm/s)	Measured ΔP (Pa)
0.09	165.89
0.14	290.19
0.21	433.66
0.27	612.51
0.33	787.62
0.39	904.44
0.45	1069.34
0.50	1239.72
0.56	1369.99

Predicted and measued pressure drop for ratio 1:60 after 24 hours mixing without particulates.

Table B84: Predicted pressure drop

Fluid velocity (cm/s)	Predicted ΔP (Pa)
0.05	89.32
0.10	181.08
0.14	275.30
0.19	371.96
0.24	471.07
0.29	572.62
0.34	676.63
0.38	783.08
0.43	891.98
0.48	1003.32
0.53	1117.12
0.57	1233.36
0.62	1352.05
0.67	1473.18
0.72	1596.76
0.77	1722.79
0.81	1851.27
0.86	1982.20
0.91	2115.57
0.96	2251.39
1.01	2389.66
1.05	2530.37

Table B85: Measured pressure drop

Fluid velocity (cm/s)	Measured ΔP (Pa)
0.09	165.89
0.14	290.19
0.21	433.66
0.27	612.51
0.33	787.62
0.39	904.44
0.45	1069.34
0.50	1239.72
0.56	1369.99
0.62	1540.37

Predicted and measued pressure drop for ratio 1:80 after one hour mixing.

Table B86: Predicted pressure drop

Fluid velocity (cm/s)	Predicted ΔP (Pa)
0.05	94.42
0.10	191.28
0.14	290.60
0.19	392.37
0.24	496.59
0.29	603.26
0.34	712.38
0.38	823.96
0.43	937.98
0.48	1054.45
0.53	1173.38
0.58	1294.75
0.62	1418.57
0.67	1544.85
0.72	1673.58
0.77	1804.75
0.81	1938.38
0.86	2074.46
0.91	2212.99
0.96	2353.97
1.01	2497.40
1.05	2643.28

Table B87: Measured pressure drop

Fluid velocity (cm/s)	Measured ΔP (Pa)
0.08	153.19
0.12	232.15
0.18	377.87
0.23	525.83
0.29	666.81
0.35	815.52
0.41	986.64
0.47	1141.08
0.53	1306.47
0.59	1451.94

Predicted and measued pressure drop for ratio 1:80 after two hours mixing.

Table B88: Predicted pressure drop

Fluid velocity (cm/s)	Predicted ΔP (Pa)
0.05	94.42
0.10	191.28
0.14	290.60
0.19	392.37
0.24	496.59
0.29	603.26
0.34	712.38
0.38	823.96
0.43	937.98
0.48	1054.45
0.53	1173.38
0.58	1294.75
0.62	1418.57
0.67	1544.85
0.72	1673.58
0.77	1804.75
0.81	1938.38
0.86	2074.46
0.91	2212.99
0.96	2353.97
1.01	2497.40
1.05	2643.28

Table B89: Measured pressure drop

Fluid velocity (cm/s)	Measured ΔP (Pa)
0.08	179.84
0.12	262.04
0.17	386.59
0.22	528.82
0.28	648.63
0.33	805.80
0.38	925.61
0.42	1065.60
0.47	1178.44
0.52	1315.19

Predicted and measued pressure drop for ratio 1:80 after 24 hours mixing.

Table B90: Predicted pressure drop

Fluid velocity (cm/s)	Predicted ΔP (Pa)
0.05	94.42
0.10	191.28
0.14	290.60
0.19	392.37
0.24	496.59
0.29	603.26
0.34	712.38
0.38	823.96
0.43	937.98
0.48	1054.45
0.53	1173.38
0.58	1294.75
0.62	1418.57
0.67	1544.85
0.72	1673.58
0.77	1804.75
0.81	1938.38
0.86	2074.46
0.91	2212.99
0.96	2353.97
1.01	2497.40
1.05	2643.28

Table B91: Measured pressure drop

Fluid velocity (cm/s)	Measured ΔP (Pa)
0.12	223.93
0.18	343.74
0.26	535.04
0.34	722.36
0.42	942.05
0.49	1132.61
0.57	1328.39
0.64	1529.65
0.71	1772.77

Predicted and measued pressure drop for ratio 1:80 after 24 hours mixing without particulates.

Table B92: Predicted pressure drop

Fluid velocity (cm/s)	Predicted ΔP (Pa)
0.05	94.42
0.10	191.28
0.14	290.60
0.19	392.37
0.24	496.59
0.29	603.26
0.34	712.38
0.38	823.96
0.43	937.98
0.48	1054.45
0.53	1173.38
0.58	1294.75
0.62	1418.57
0.67	1544.85
0.72	1673.58
0.77	1804.75
0.81	1938.38
0.86	2074.46
0.91	2212.99
0.96	2353.97
1.01	2497.40
1.05	2643.28

Table B93: Measured pressure drop

Fluid velocity (cm/s)	Measured ΔP (Pa)
0.12	223.93
0.18	343.74
0.26	535.04
0.34	722.36
0.42	942.05
0.49	1132.61
0.57	1328.39
0.64	1529.65
0.71	1772.77
0.78	1987.73

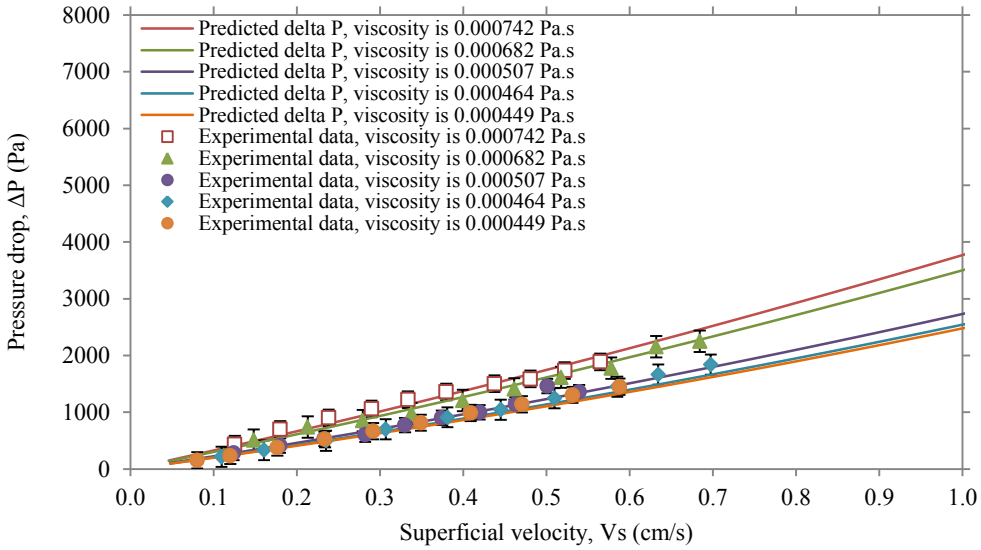

Figure B1: Pressure drop- Superficial velocity relationship after one hour mixing

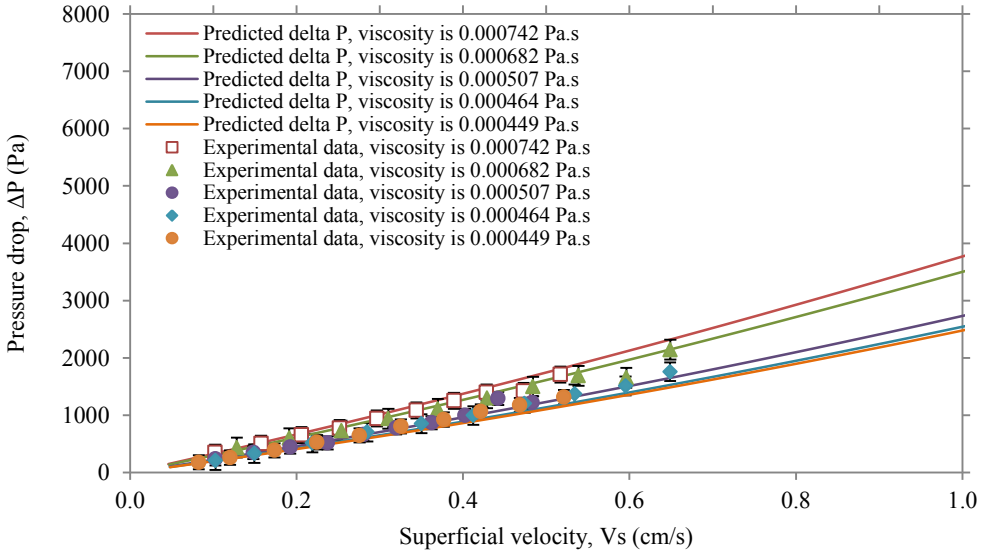

Figure B2: Pressure drop- Superficial velocity relationship after two hours mixing

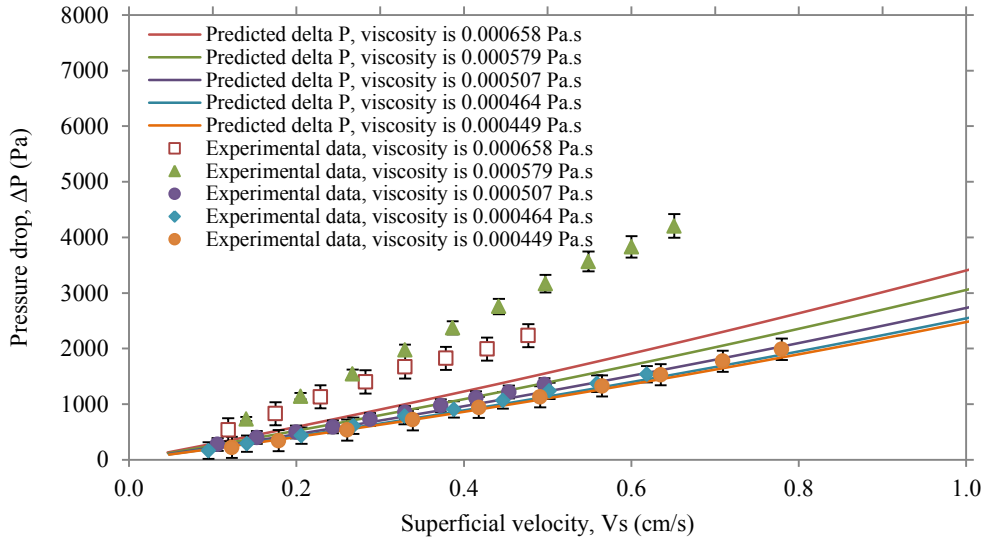

Figure B3: Pressure drop- Superficial velocity relationship after 24 hours mixing

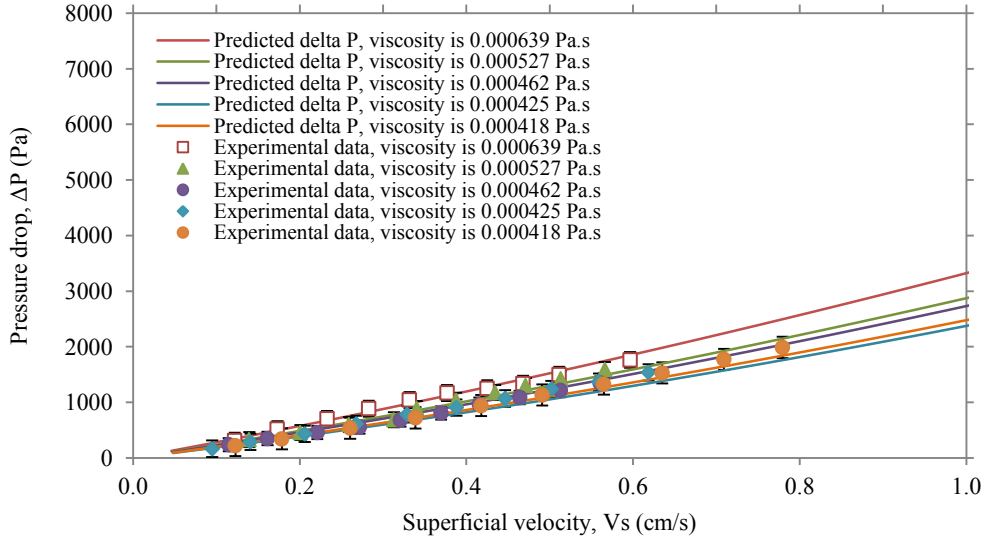

Figure B4: Pressure drop- Superficial velocity relationship after 24 hours mixing without particulates.

Appendix C

- **Fluidization**

When a fluid is passed upwards through a bed of particles the pressure loss in the fluid due to frictional resistance increases with increasing fluid flow. When the upward drag force exerted by the fluid on the particles is equal to the apparent weight of particles in the bed, the particles are lifted by the fluid, and the bed becomes fluidized.

The force balance across the fluidized bed dictates that the fluid pressure loss across the bed of particles is equal to the apparent weight of the particles per unit area of the bed. So, for a randomly packed bed with cross-sectional area A, particle density ρ_s, fluid density ρ_f, length of L, and porosity of ε, the incipient pressure drop would be:

$$\Delta P = L(1-\varepsilon)(\rho_p - \rho_f)g$$

A plot of fluid pressure loss across the bed versus superficial fluid velocity through is shown in the following figure.

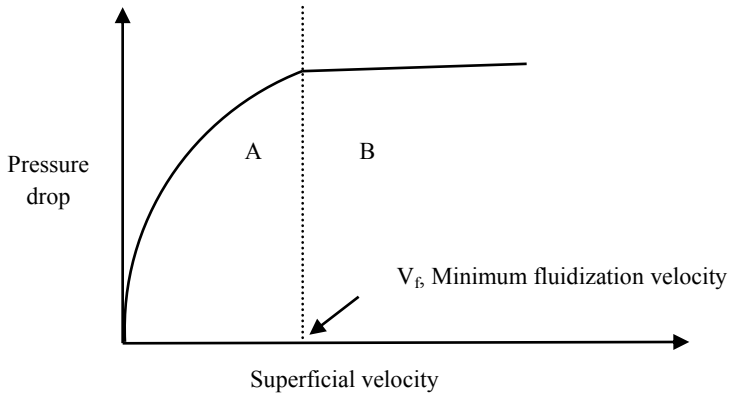

Figure C 1: Pressure drop-Superficial velocity relationships

The Figure C2 illustrates in region A the solid particles do not move. The pressure loss versus fluid velocity relationship in this region is described by the Carman–Kozeny equation in the laminar flow regime and the Ergun equation in general.

The superficial fluid velocity at which the packed bed becomes a fluidized bed is known as the minimum fluidization velocity or incipient fluidization velocity (v_f). It will increase with particle size and particle density and is affected by fluid properties. It is possible to derive an expression for V_f by equating the expression for pressure loss in a fluidized bed with the expression for pressure loss across a packed bed.

Typically, for a bed of small particles ($D_p \leq 0.1$ mm) and the flow conditions at the laminar regime (Reynolds number is relatively smaller than 10), the Kozeny-Carman equation, applicable to the viscous flow regime, for establishing the point of onset of fluidization.

$$V_f = \frac{(\rho_p - \rho_f) g D_p^2}{150\,\mu} \frac{\varepsilon^3}{(1-\varepsilon)}$$

When the superficial velocity is equal to V_f, incipient fluidization will happen.

For large particles ($D_p \geq 1$mm), inertial effects are important, and the full Ergun equation must be used to determine V_f [46, 48, 49].

$$V_f = -\frac{42.8\,\mu\,(1-\varepsilon)}{\rho_f D_p} + \sqrt{\left(\frac{42.8\,\mu\,(1-\varepsilon)}{\rho_f D_p}\right)^2 + \frac{0.57\,(\rho_p - \rho_f)}{\rho_f} g D_p \varepsilon^3}$$

- **Comparison between predicted incipient fluidization velocity and maximum measured superficial velocity; also, comparison between predicted incipient pressure drop and maximum measured pressure drop.**

Table C1 to C4 show the comparison between predicted and maximum measured values for incipient fluidization velocity and pressure drop for all solutions at 1, 2, , 24 hours after mixing, and 24 hours after mixing without asphaltene precipitate. For all ratios in different hour of mixing, the predicted incipient fluidization velocity is in range of 1.0 to 1.4 cm/s and maximum measured superficial velocity is in range of 0.5 to 0.7 cm/s. Also, predicted incipient fluidizing pressure drop is in range of 3611 to 3665 Pa·s and maximum measured pressure drop is in range of 1350 to 2150 Pa·s, so the superficial velocity for all samples was kept in half of the predicted incipient fluidization velocity range, and pressure drop that we are dealing with is in half of the predicted fluidizing pressure drop range.

Table C1: Bitumen-heptane (g/g) after one hour mixing

Bitumen-heptane (g/g)	viscosity of mixture (Pa·s)	density of mixture (kg/m^3)	Maximum measured V_S (cm/s)	Predicted Incipient V_F (cm/s)	Maximum measured ΔP (Pa)	Predicted Incipient fluidising ΔP (Pa)
1:80	0.000449	686.33	0.59	1.4	1451.9	3665.0
1:60	0.000464	687.24	0.69	1.3	1838.5	3663.3
1:20	0.000507	689.6	0.54	1.3	1357.8	3658.9
1:10	0.000682	704.29	0.68	1.0	2249.3	3631.5
1:5	0.000742	715.01	0.56	1.0	1888.8	3611.5

Table C2: Bitumen-n-heptane (g/g) after two hours mixing

Bitumen-heptane (g/g)	viscosity of mixture (Pa·s)	density of mixture (kg/m^3)	Maximum measured V_S (cm/s)	Predicted Incipient V_F (cm/s)	Maximum measured ΔP (Pa)	Predicted Incipient fluidising ΔP (Pa)
1:80	0.000449	686.33	0.52	1.4	1315.2	3665.0
1:60	0.000464	687.24	0.65	1.3	1759	3663.3
1:20	0.000507	689.6	0.48	1.3	1221.8	3658.9
1:10	0.000682	704.29	0.65	1.0	2143.2	3631.5
1:5	0.000742	715.01	0.52	1.0	1709.5	3611.5

Table C3: Bitumen-n-heptane (g/g) after 24 hours mixing

Bitumen-heptane (g/g)	viscosity of mixture (Pa·s)	density of mixture (kg/m3)	Maximum measured V_S (cm/s)	Predicted Incipient V_F (cm/s)	Maximum measured ΔP (Pa)	Predicted Incipient fluidising ΔP (Pa)
1:80	0.000449	686.33	0.78	1.4	1987.7	3665.0
1:60	0.000464	687.24	0.62	1.3	1540.4	3663.3
1:20	0.000507	689.6	0.50	1.3	1352.5	3658.9
1:10	0.000579	704.29	0.65	1.2	4026.4	3631.5
1:5	0.000658	715.01	0.57	1.1	3773.9	3611.5

Table C4: Bitumen-n-heptane (g/g) after 24 hours mixing without asphaltene

Bitumen-heptane (g/g)	viscosity of mixture (Pa·s)	density of mixture (kg/m3)	Maximum measured V_S (cm/s)	Predicted Incipient V_F (cm/s)	Maximum measured ΔP (Pa)	Predicted Incipient fluidising ΔP (Pa)
1:80	0.000418	686.33	0.71	1.4	1772.8	3665.0
1:60	0.000425	687.24	0.55	1.3	1370	3663.3
1:20	0.000462	689.6	0.56	1.3	1349.3	3658.9
1:10	0.000538	704.29	0.56	1.2	1591.9	3631.5
1:5	0.000639	715.01	0.59	1.1	1764.3	3611.5